High-Energy Neutrino Propagation in Matter

V. Naumov

JINR, Dubna, Dipartimento di Fisica & INFN, Firenze

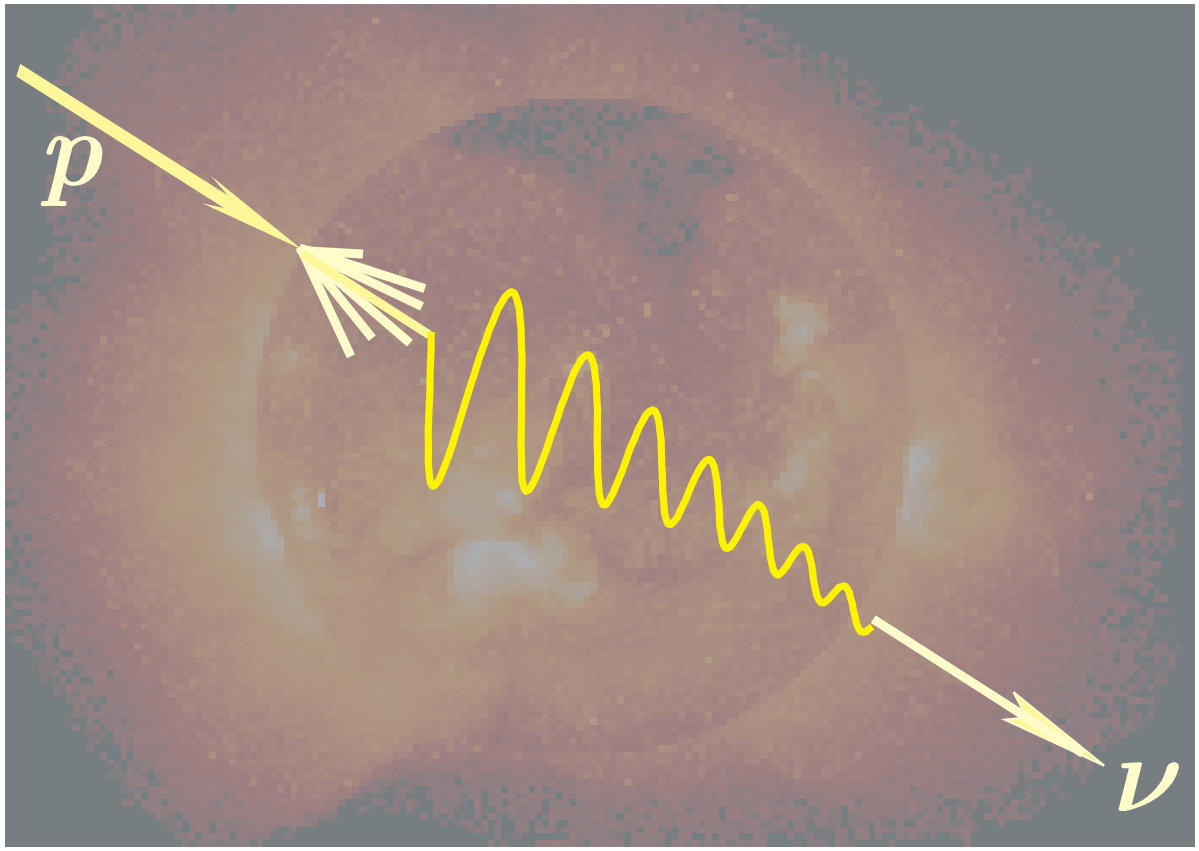

Astrophysical sources of high-energy neutrinos

Candidate point sources

- ⋆ **Young supernova remnants**
  [due to CR acceleration by shock waves from SN explosions]
- ⋆ **Accreting neutron stars and black holes**
- ⋆ **Binary (multiple) systems**
  [pulsar + giant, pulsar + star filling its Roche lobe, white dwarf + (super)giant, etc.]
- ⋆ **The Galactic center**
  [within the model of a supermassive accreting black hole]
- ⋆ **Active Galactic Nuclei (AGNs)**
  [Seyfert galaxies, N galaxies, quasars, Lacertae (BLLac objects), blazars (radio-loud AGNs); particle acceleration in extragalactic jets from radio-quiet and radio-loud AGNs]
- ⋆ **Gamma-Ray Bursts (GRBs)**
  [example: γ's and ν's arise from decay of pions produced in shock front collisions]
- ⋆ **Hidden or latent sources**
  [young SN shell, cocooned massive black hole (MBH) in AGN, Thorne–Żytkow star (the binary with a neutron star submerged into a red supergiant core), AGN with standing shock in the vicinity of a MBH, etc.]

Diffuse neutrino backgrounds

- ⋆ **Galactic neutrinos**
  [including ν's from CR interactions with the spherical halo of baryonic dark matter]
- ⋆ **Quasi-diffuse background from AGN's**
- ⋆ **Neutrinos from intergalactic space**
  [the most important are UHE ν's from the CR spectrum tail (GZK cutoff)]
- ⋆ **Pregalactic neutrinos and neutrinos from the bright phase of galaxy evolution**

Speculative sources of the highest-energy neutrinos and science fiction

- ⋆ **Topological defects**
  [ultra-heavy particle emission and acceleration by saturated superconducting cosmic strings, cusp radiation from ordinary cosmic strings, vortons, textures, global monopoles, etc.]
- ⋆ **Mini-black-hole evaporation**
- ⋆ **Decay of super-heavy exotic particles** [such as long-lived Big Bang relics or the Planck mass objects (planckeons $\sim$ fridmons $\sim$ maximons $\sim$ cosmions)]
- ⋆ and many many others...

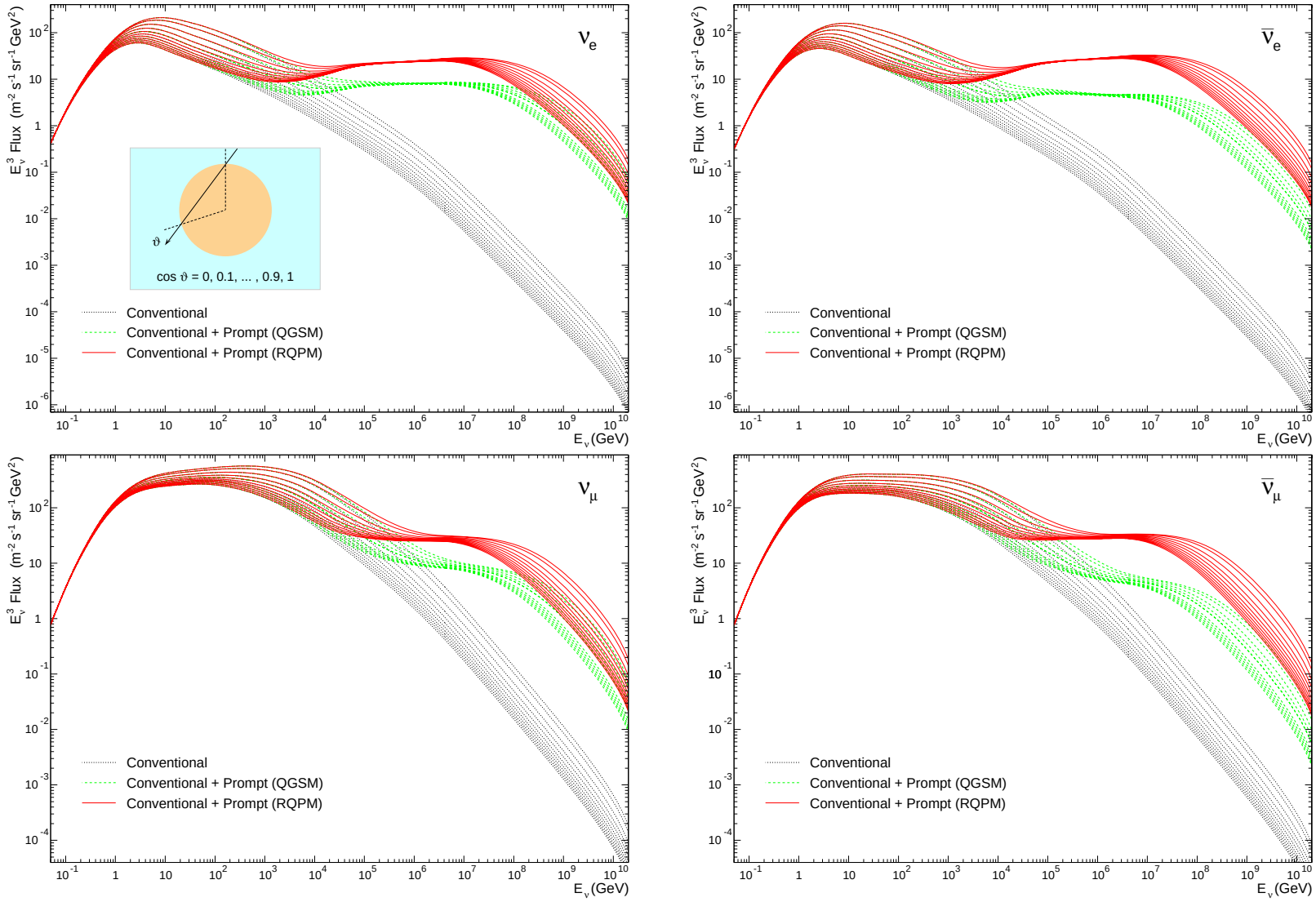

Figure 1: Energy spectra of downward-going atmospheric (anti)neutrinos for 11 zenith angles with $\cos\theta$ varied from 0 to 1 with an increment of 0.1. The range below several GeVs is for Kamioka site.

Explanation to Fig. 2 (next slide)

Shaded regions

- **Cerulean band:** terrestrial atmosphere in the horizontal (upper boundary) and vertical (lower boundary) directions including prompt neutrinos from charm production [Thunman *et al.* (1996)];
- **Yellow band:** Galactic disk towards the center (upper boundary) and the poles (lower boundary) from [Thunman *et al.* (1996)];
- **Gray area:** unresolved extragalactic sources from which gamma rays and cosmic-ray nucleons escape freely (curved upper boundary) and from which only gamma rays escape (straight upper boundary) [Mannheim *et al.* (1999)], cosmic-ray storage in galaxy clusters (lower boundary) [Colafrancesco & Blasi (1998)].

Numbered lines

1 – Nellen *et al.* (1993) model for pp interactions in the core of AGN;

2 – Stecker & Salamon (1996) model for $p\gamma$ interactions in the core of AGN (from which nucleons can not freely escape);

3 – Mannheim *et al.* (1999) maximum model for $p\gamma$ interactions in extragalactic sources;

4 – Mannheim (1995) model A for $p\gamma$ interactions in blazar jets producing UHECRs through neutron escape;

5 – $p\gamma$ interactions due to UHE cosmic rays escaping from radio galaxies and traveling through the 2.7 K background according to the model of Rachen & Biermann (1993,1996);

6 – pp interactions in host galaxies of blazar jets as assumed in the model of Mannheim (1995);

7 – GRB model by Waxman & Bahcall (1997);

8 – decaying XY gauge bosons of mass 10^{16} GeV created at topological defects as in the models of Sigl (1998) and Birkel & Sarkar (1998).

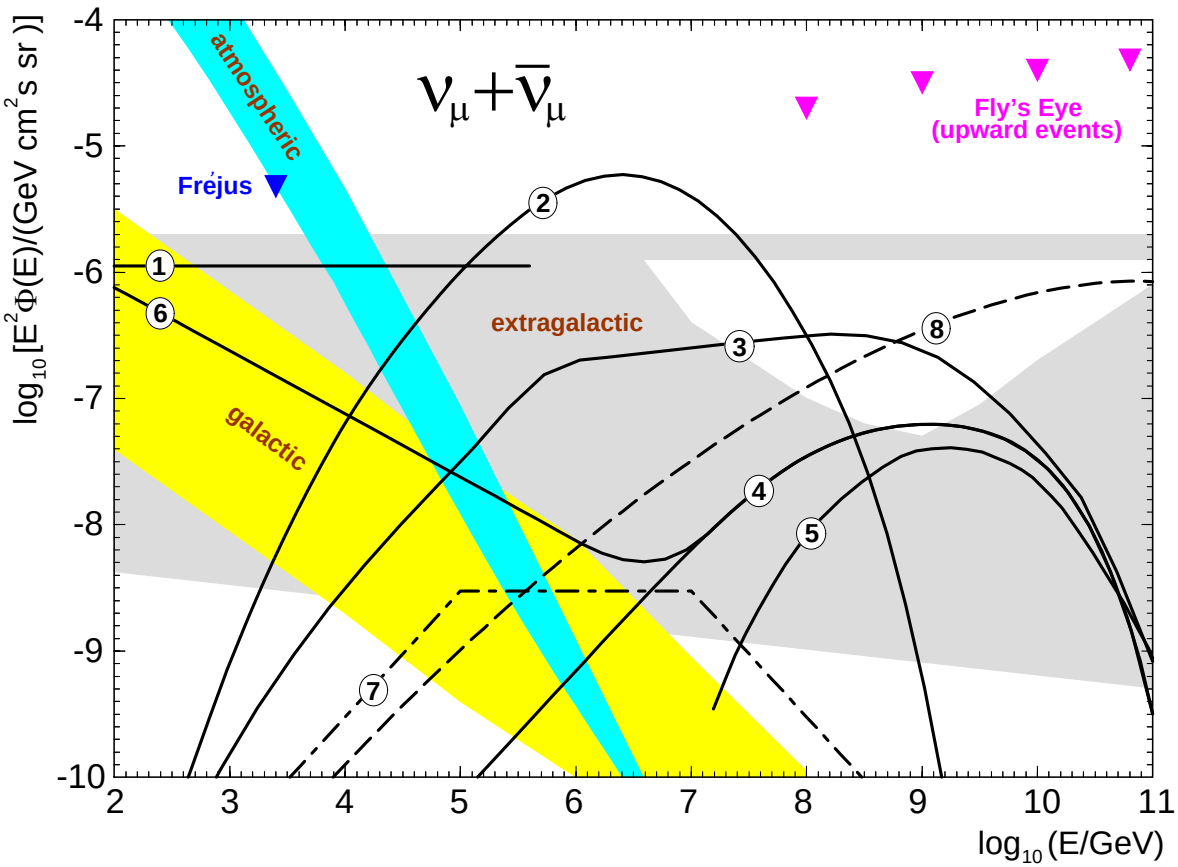

Figure 2: Summary of expected $\nu_\mu + \overline{\nu}_\mu$ intensities for diffuse emission from various sources. The experimental data (triangles) are from Frejús proton decay detector (limit on any excess above the atmospheric background) and Fly's Eye fluorescence air shower detector (limits on upward events).
[From J. G. Learned and K. Mannheim, Ann. Rev. Nucl. Part. Sci. **50** (2000) 679, Fig. 8.]

Explanation to Fig. 3 (next slide)

Numbered lines

1 – Nellen *et al.* (1993) model for the core emission from 3C273 due to pp interactions (or similarly Mrk501 during its outburst in 1997 if it emits half of its TeV gamma ray flux in neutrinos);

2 – Stecker & Salamon (1996) model for the core emission from 3C273 due to $p\gamma$ interactions;

3 – Mannheim (1993) model for the relativistic jet of 3C273 including pp and $p\gamma$ interactions;

4 – Coma cluster according to the model of Colafrancesco & Blasi (1998);

5 – Crab nebula, Model I due to Bednarek & Protheroe (1997);

6 – cosmic-ray induced neutrinos from the sun according to Ingelman & Thunman (1996);

7 – supernova remnant IC444 according to the model of Gaisser *et al.* (1998);

8 – supernova remnant γ Cygni according to Gaisser *et al.* (1998);

9 – CasA according to the model of Atoyan *et al.* (2000) (adopting $L_\nu = L_\gamma$ and $E_\nu = 0.5 E_\gamma$).

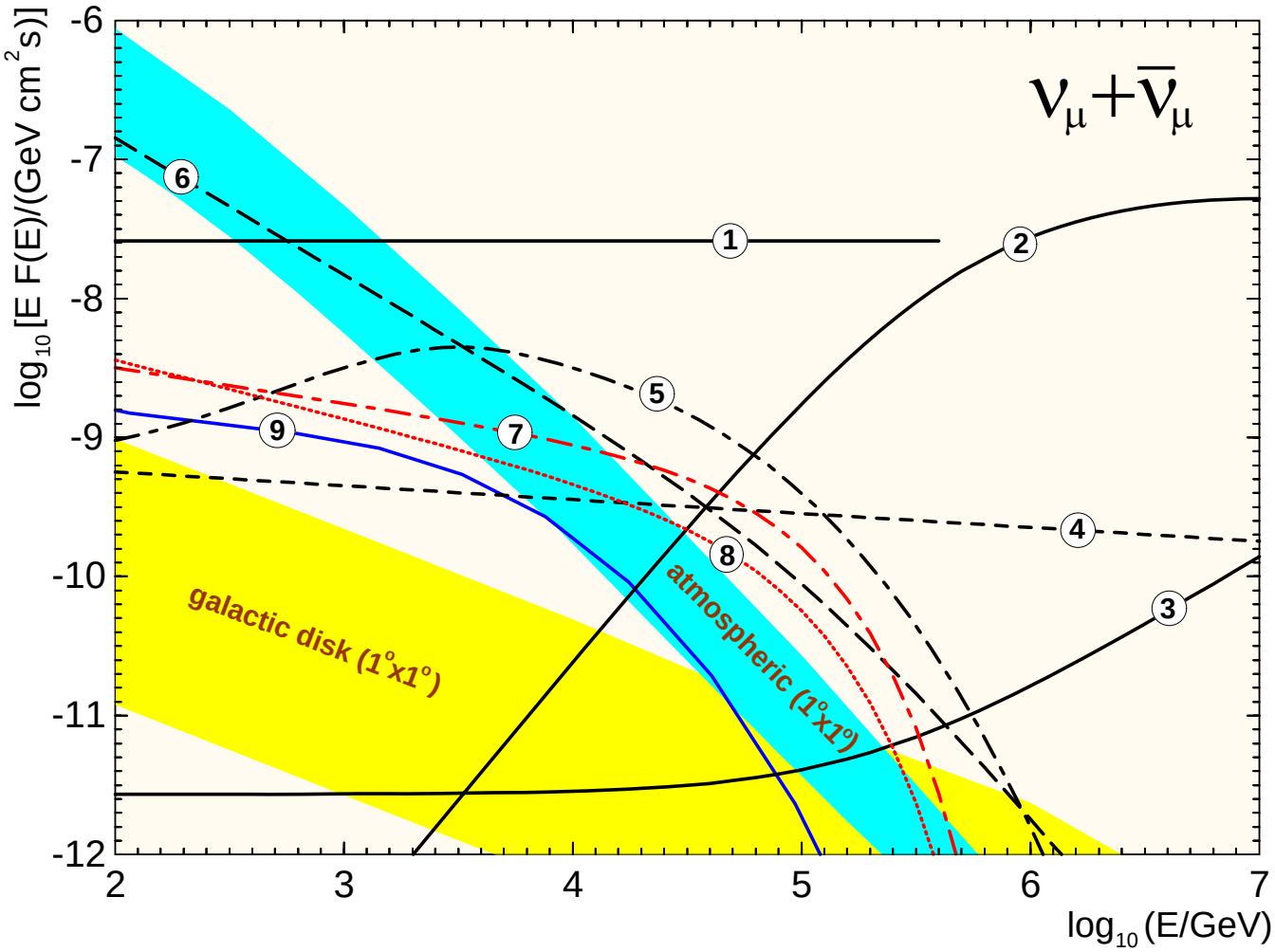

Figure 3: Summary of expected $\nu_\mu + \overline{\nu}_\mu$ from candidate cosmic-ray accelerators ("point sources").
[From J. G. Learned and K. Mannheim, Ann. Rev. Nucl. Part. Sci. **50** (2000) 679, Fig. 10.]

Figure 4: The third-brightest star of Cygnus, called γ Cygni or Sadr (the bright star near the center of the photo), surrounded by a huge complex of emission nebulosity.
[From Gallery of Astrophotography & CCD Images, URL: <http://www.astro.univie.ac.at/~exgalak/koprolin/Photo/>.]

According to L. A. Anchordoqui *et al.*, the **Cygnus** region (Cygnus X-3 or Cygnus-OB2 cluster) may be a source of HE free neutrons created via nuclei photo-disintegration on background photon fields. The neutron β decay provides detectable $\overline{\nu}$ flux:

$$n \to p + e^- + \overline{\nu}_e,$$

$$\left[L_\odot^{\rm osc} \sim 0.01 \left(\frac{E_\nu}{\rm PeV} \right) \ {\rm ps}, \ \ \theta_\odot \simeq 32.5^\circ \right]$$

$$\overline{\nu}_e \overset{\text{vacuum}}{\rightsquigarrow} 0.6\,\overline{\nu}_e + 0.2\,\overline{\nu}_\mu + 0.2\,\overline{\nu}_\tau.$$

Figure 5 shows the integrated $\overline{\nu}_\mu$ and $\overline{\nu}_\mu + \overline{\nu}_e + \overline{\nu}_\tau$ fluxes predicted to arrive at Earth from the direction of the Cygnus. The expected rates of $\overline{\nu}_\mu$ and $\overline{\nu}_\mu + \overline{\nu}_e + \overline{\nu}_\tau$ induced showers to be detected in the **IceCube** (the planned angular resolution is about 0.7°) together with the expected background for the same angular bin are plotted on the bottom-left.

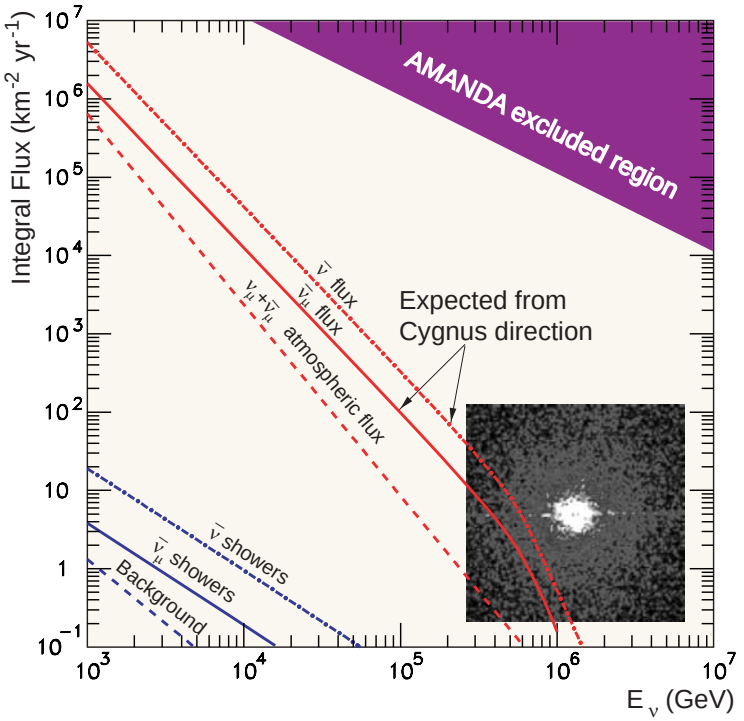

Figure 5: Antineutrino fluxes from Cygnus. The integrated AN flux is shown for an angular bin of $1^\circ \times 1^\circ$. The excluded region is according to J. Ahrens *et al.*, Phys. Rev. Lett. **92** (2004) 071102 (astro-ph/0309585). [The data are borrowed from L. A. Anchordoqui *et al.*, Phys. Lett. B **593** (2004) 42–47 (astro-ph/0311002). The Cygnus X-3 image by the Chandra X-ray Observatory is taken from URL <http://www.mfsc.nasa.gov/>.]

Using the Sun as a standard candle for the calibration of neutrino detectors is hampered by the rather low expected event rate which is ~ 17 per year in a cubic-kilometer NT above 100 GeV. If the rate were higher than predicted, this could indicate neutralino annihilation in the solar interior. Thus, in spite of the low CR induced flux, it is desirable to obtain statistics of solar HE ν's down to this conservative flux.

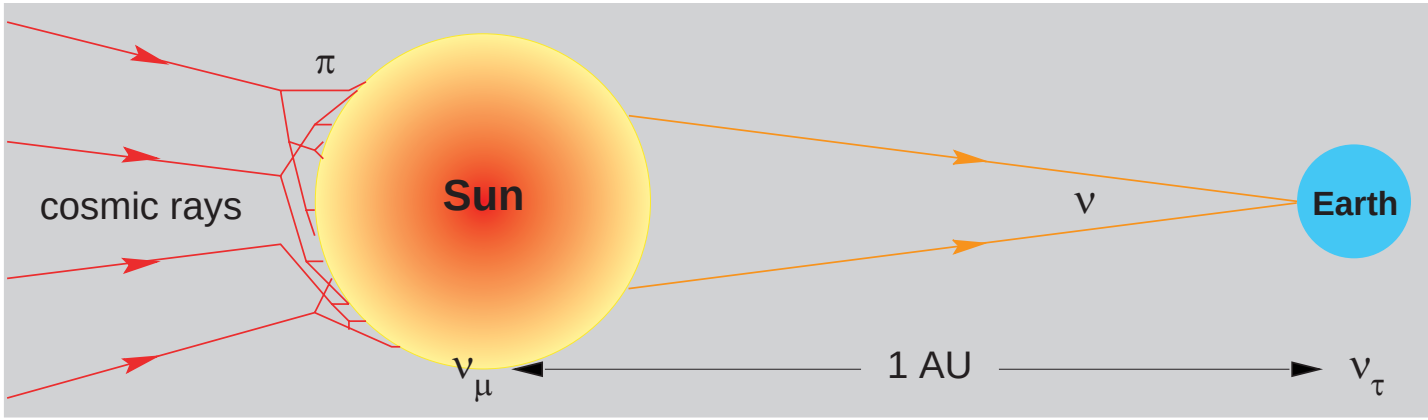

Figure 6: Cosmic rays hitting the Sun produce ν_μ's which propagate further to Earth. At an energy of 10 TeV the length for $\nu_\mu \leftrightarrow \nu_\tau$ oscillations is (according to the SK AN result) about 1 AU.
[From J. G. Learned and K. Mannheim, Ann. Rev. Nucl. Part. Sci. **50** (2000) 679, Fig. 7.]

Particular interest lies in a likely $\nu_\mu \leftrightarrow \nu_\tau$ oscillations for which the computed rate is 4–6 τ's above 100 GeV per year in a 1 km^3 detector [Hettlage *et al.* (2000)]. It is of the same order of magnitude as the expected τ rate in the CERN–NGS experiment).

Detectors for high-energy neutrino astronomy

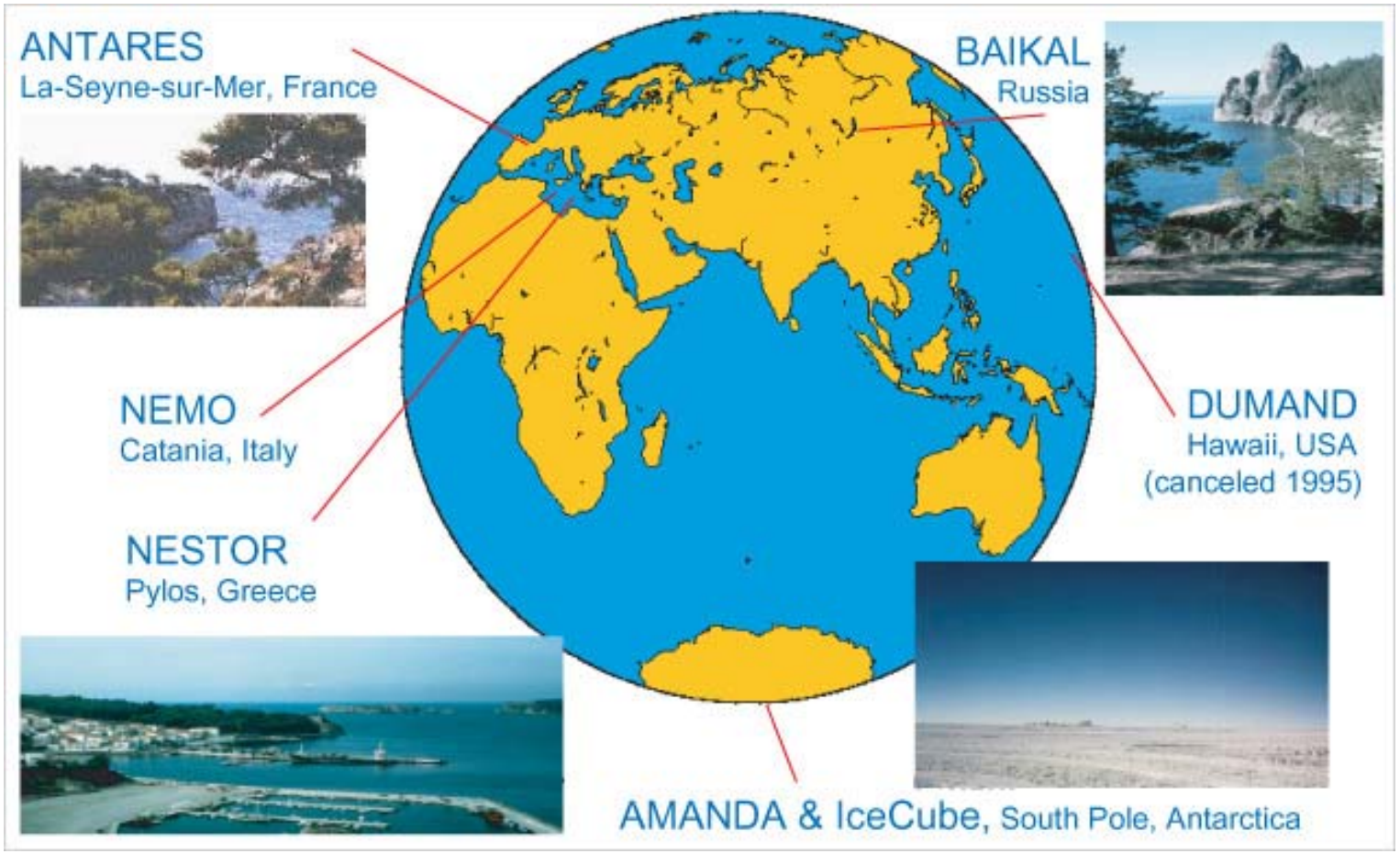

Figure 7: A map of underwater/ice Cherenkov neutrino telescope projects.

Table 1: Present status of underwater/ice Cherenkov neutrino telescope projects.

Lab/Location/Stage	Year(s)	Sensitive area* (10^3 m^2)	Status (fall, 2003)
DUMAND I, II *Pacific near Hawaii Big Island; at a depth of ~4.5 km*	Historically first underwater project. Closed down...**		
BAIKAL NT *Lake Baikal, East Siberia; at a depth of about 1.1. km*			
NT-36	1993-95	0.15-0.20	Stepwise deployment & going into operation
NT-72	1995-96	0.4-3.0	
NT-96	1996-97	0.8-6.0	
NT-144	1997-98	1.0-8.0	
NT-200	1998	2.0-10.0	Operates
AMANDA *South Pole; at a depth of 0.8 to 2 km*			
AMANDA A	1994	Small	Stepwise deployment & going into operation
AMANDA A	1996	1.0	
AMANDA B4	1998	5-6	
AMANDA II	2000	30-50	Operates
AMANDA KM3 or IceCube	2005	1000	Under construction
NESTOR *Ionian Sea near Pylos, Peloponnesos, Greece; at a depth of about 3.8 km*	2004 ?	1st phase: 20 KM^3 in prospect	Under construction & test
ANTARES *Mediterranean near Toulon, France; at a depth from 2.4 to 2.7 km (the most appropriate site is identified)*	2004 ?	to 100-200 KM^3 in prospect	R & D
NEMO *Capo Passero (Sicily), Italy; at a depth of about 3.4 km*	?	to 3500 KM^3 in prospect	R & D

* The sensitive area (SA) enlarges with muon energy, e.g. the estimated SA of the Baikal NT-200 is ~ 2300 m^2 (~ 8500 m^2) for 1-TeV (100-TeV) μ's.

** Some 1-string prototypes of the DUMAND array were and several useful results were obtained.

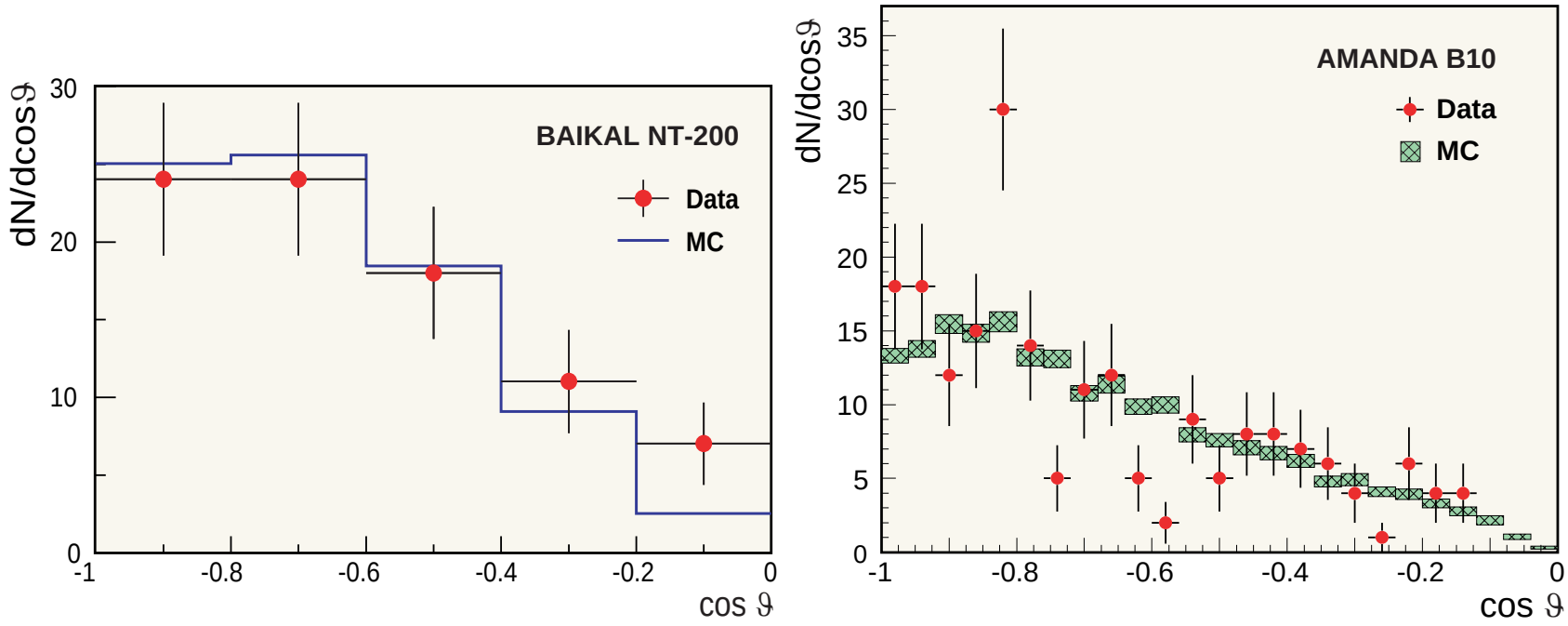

Figure 8: Zenith angle distributions of upward-going reconstructed events.
Left panel: 84 Baikal NT-200 events and simulated distribution of upward muon tracks due to atmospheric neutrinos (80.5 predicted events).
Right panel: 204 AMANDA-B10 and Monte Carlo simulated distribution of upward muon tracks due to atmospheric neutrinos. The size of the hatched boxes indicates the statistical precision of the AN flux simulation. The MC prediction is normalized to the data.
[From R. Wischnewski (for the Baikal Coll.), contribution to the 28th ICRC, Tsukuda, Japan, July 31 – August 7, 2003 (astro–ph/0305302); J. Ahrens *et al.* (AMANDA Coll.), Phys. Rev. D **66** (2002) 012005 (astro–ph/0205109).]

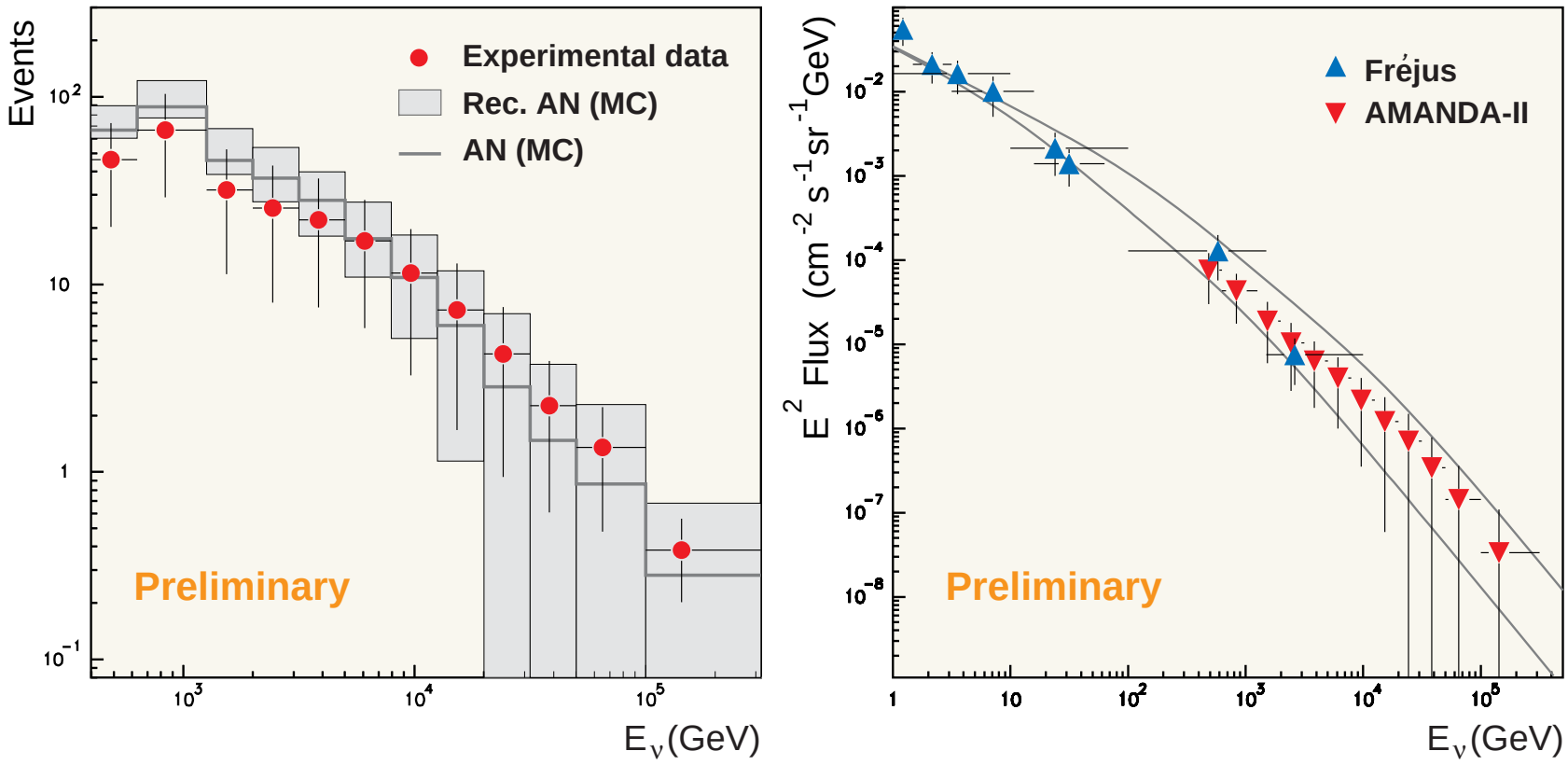

Figure 9: Recorded events and reconstructed muon neutrino energy spectrum in AMANDA-II.
Left panel: on filter level, energy distribution of atmospheric neutrino expectation (solid), unfolded energy distribution of AN from Monte Carlo (boxes), reconstracted data (points).
Right panel: reconstructed neutrino flux compared to Fréjus data and the AN flux expectation.
[From H. Geenen (for the AMANDA Coll.), contribution to the 28th ICRC, Tsukuda, Japan, July 31 – August 7, 2003 (see also the AMANDA Berkeley Group URL <http://area51.berkeley.edu/>).]

Classical transport through dense media

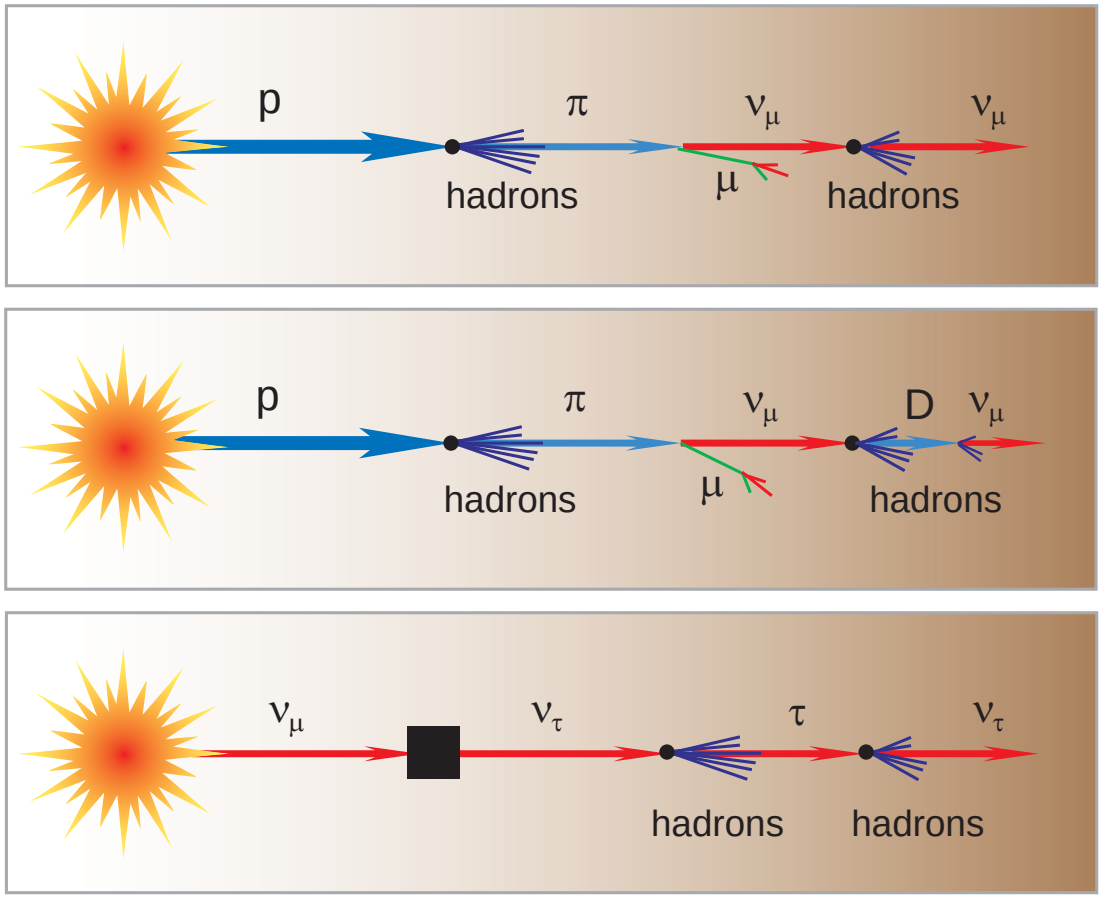

Figure 10: Primitive schemes for neutrino production, absorption and regeneration in matter.

Why is dense medium somewhat simpler than rarefied?

In *dense enough matter*, the main regeneration mechanism is the NC induced energy loss with no change of flavor:

$$\nu_\ell + N \to \nu_\ell + X, \quad \overline{\nu}_\ell + N \to \overline{\nu}_\ell + X \quad (\ell = e, \mu, \tau).$$

The NC scattering off electrons is usually unimportant with the only exception (for a normal C asymmetric matter) for $\overline{\nu}$ which can effectively regenerate (*in very narrow energy range*) through the reaction

$$\overline{\nu}_e e^- \to \overline{\nu}_e e^-.$$

This is a particular case because of the W boson resonance formed in the neighborhood of $E_\nu^{\text{res}} = m_W^2/2m_e \approx 6.33\,\text{PeV}$.

Under certain conditions, neutrinos may transform, changing energy and/or flavor via processes like

$$\overline{\nu}_e e^- \to \overline{\nu}_\ell \ell^- \quad \text{or} \quad \nu_\ell e^- \to \nu_e \ell^-.$$

an owing to production and decay of unstable hadrons.[a]

[a] In exotic media (as in *hot* galactic haloes filled with massive neutrinos) neutrinos can chane flavor through the reaction chains like

$$\nu_\mu \overline{\nu}_\tau \to \mu^- \tau^+, \quad \tau^+ \to \overline{\nu}_\tau X, \text{ etc.}$$

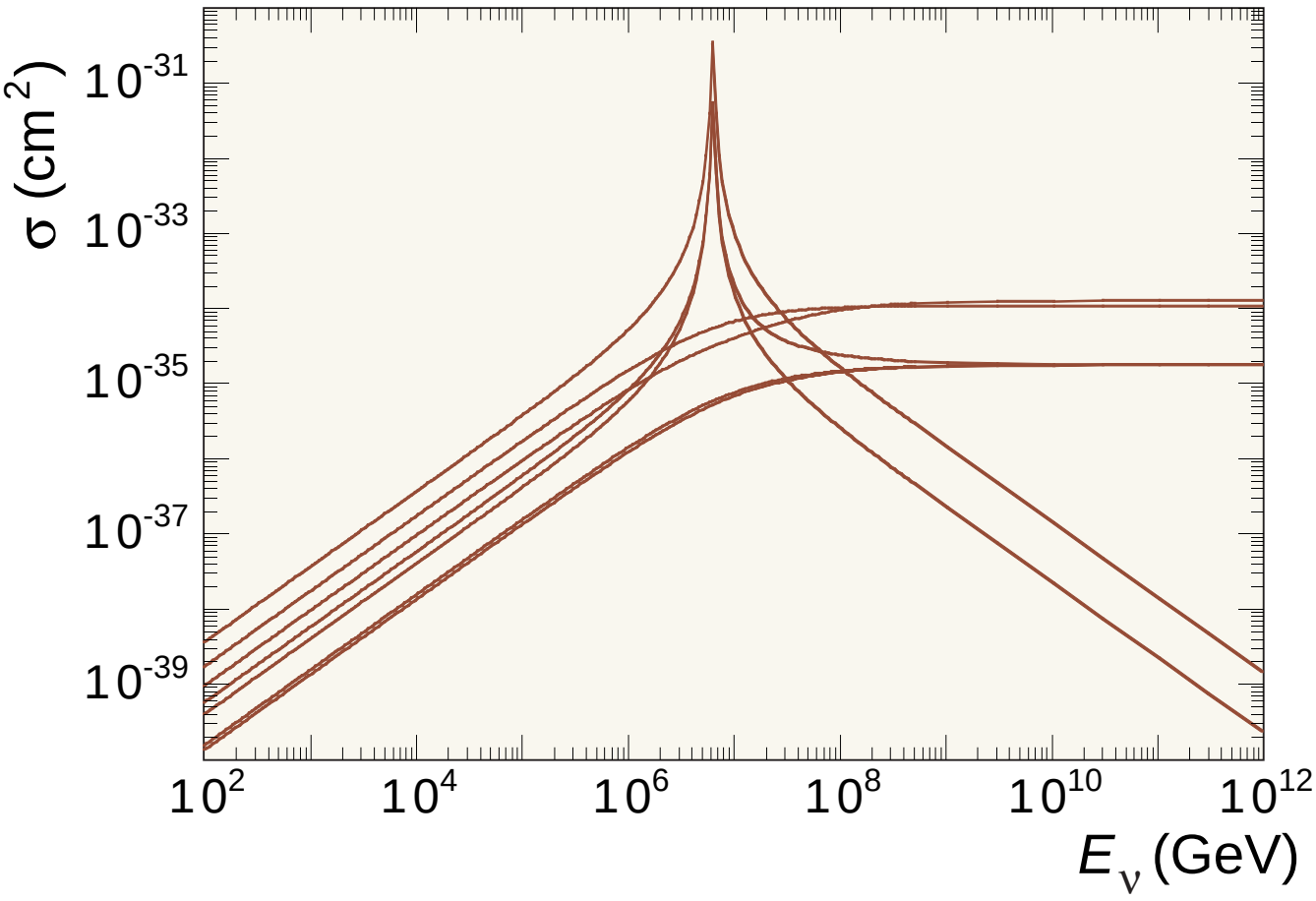

Figure 11: Total cross sections for neutrino interactions on electron targets. At low energies, from largest to smallest cross section, the processes are (i) $\overline{\nu}_e e \to$ hadrons, (ii) $\nu_\mu e \to \mu \nu_e$, (iii) $\nu_e e \to \nu_e e$, (iv) $\overline{\nu}_e e \to \overline{\nu}_\mu \mu$, (v) $\overline{\nu}_e e \to \overline{\nu}_e e$, (vi) $\nu_\mu e \to \nu_\mu e$, (vii) $\overline{\nu}_\mu e \to \overline{\nu}_\mu e$.
[From R. Gandhi et al., Astropart. Phys. **5** (1996) 81 (hep–ph/9512364).]

Table 2: Integrated cross sections for neutrino–electron and neutrino–nucleon scattering at $E_\nu = m_W^2/2m_e \approx 6.33\,\text{PeV}$. [From R. Gandhi et al., Astropart. Phys. **5** (1996) 81 (hep–ph/9512364).]

Reaction	σ (cm^2)	Reaction	σ (cm^2)
$\nu_\mu e \to \nu_\mu e$	5.86×10^{-36}	$\nu_\mu N \to \mu^- +$ anything	1.43×10^{-33}
$\overline{\nu}_\mu e \to \overline{\nu}_\mu e$	5.16×10^{-36}	$\nu_\mu N \to \nu_\mu +$ anything	6.04×10^{-34}
$\nu_\mu e \to \mu \nu_e$	5.42×10^{-35}	$\overline{\nu}_\mu N \to \mu^+ +$ anything	1.41×10^{-33}
$\nu_e e \to \nu_e e$	3.10×10^{-35}	$\overline{\nu}_\mu N \to \overline{\nu}_\mu +$ anything	5.98×10^{-34}
$\overline{\nu}_e e \to \overline{\nu}_e e$	5.38×10^{-32}		
$\overline{\nu}_e e \to \overline{\nu}_\mu \mu$	5.38×10^{-32}		
$\overline{\nu}_e e \to \overline{\nu}_\tau \tau$	5.38×10^{-32}		
$\overline{\nu}_e e \to$ hadrons	3.41×10^{-31}		
$\overline{\nu}_e e \to$ anything	5.02×10^{-31}		

Just at the resonance peak, $\sigma^{\text{tot}}_{\overline{\nu}_e e} \approx 250\, \sigma^{\text{tot}}_{\overline{\nu}_e N}$.

Regeneration in hadronic cascades

This mechanism can play a role if the column depth of the medium exceeds the neutrino interaction length,

$$h \gtrsim \lambda_\nu^{\rm in}(E),$$

while the average density ($\langle\rho\rangle$) is low enough (like in the Thorne–Żytkow objects):

$$\langle\rho\rangle \lesssim \rho_k^0 \left[\frac{\lambda_k^{\rm in}(E_k)}{45\ {\rm g/cm^2}}\right]\left[\frac{1\ {\rm PeV}}{E_k}\right].$$

Here $\lambda_k^{\rm in}(E_k)$ is the inelastic scattering length for a hadron k of energy $E_k = \xi_k E$ at production ($45\,{\rm g/cm^2}$ is the typical value for a hydrogen-helium matter background), ξ_k is the average fraction of the incident neutrino energy E carried by the hadron,

$$\rho_k^0 \approx \begin{cases} (0.8-6.0)\times 10^{-8}\,{\rm g/cm^3} & \text{for } k=\pi^\pm, K_L^0, K^\pm, \\ 1.4\times 10^{-2}\,{\rm g/cm^3} & \text{for } k=D^\pm, D^0, \overline{D}^0, \Lambda_c^\pm. \end{cases}$$

Generally, this mechanism is not-too-effective because $\xi_k \ll 1$. However

- it becomes important for flat ν spectra, like ones expected from topological defects;
- regeneration due to neutrinoproduction and decay of charmed particles may be of some effect for HE neutrinos propagating through the solar interior.

Muon neutrino regeneration through CC induced chains

The charged-current induced chains

$$\nu_\mu N \to \mu^- X, \quad \mu^- \to \nu_\mu \overline{\nu}_e e^- \quad \text{and} \quad \overline{\nu}_\mu N \to \mu^+ X, \quad \mu^+ \to \nu_\mu \nu_e e^+$$

are much more effective if only

$$\langle \rho \rangle \lesssim 6.4 \times 10^{-7} \left[\frac{2.5 \times 10^{-6}\ \mathrm{cm^2 g^{-1}}}{b_\mu(E_\mu)} \right] \left[\frac{1\ \mathrm{PeV}}{E_\mu} \right] \frac{\mathrm{g}}{\mathrm{cm}^3}, \tag{1}$$

where b_μ is the muon fractional energy loss due to radiative and photonuclear interactions, a slowly varying function of muon energy $E_\mu = \xi_\mu E$ and $\xi_\mu \sim 1$. Elementary considerations suggest that

under condition (1)*, even very thick layers of matter never become opaque to muon neutrinos and antineutrinos.*

Note:

The form of distributions of density and composition of the medium also affects the neutrino yields from decay of hadrons and muons. As a result, the regeneration effect may be very different for neutrino beams penetrating the same *nonuniform* medium in different directions.

Tau neutrino regeneration through CC induced chains

HE and UHE ν_τ and $\overline{\nu}_\tau$ effectively regenerate (losing energy) even in *rather dense media*, through the charged-current reaction chain

$$\nu_\tau N \to \tau X, \quad \tau \to \nu_\tau X.$$

Indeed, the corresponding "critical" density can be roughly estimated as

$$2 \times 10^4 \left[\frac{10^{-8}\ \mathrm{cm^2 g^{-1}}}{b_\tau(E_\tau)}\right] \left[\frac{1\ \mathrm{PeV}}{E_\tau}\right] \frac{\mathrm{g}}{\mathrm{cm}^3} \qquad (E_\tau = \xi_\tau E \sim E).$$

The Earth is therefore effectively transparent for ν_τ and $\overline{\nu}_\tau$ at energies up to 1-10 EeV.

This fact is very profitable for future experiments with underwater NTs (e.g., detecting ν_τ events from astrophysical neutrino oscillations at energies $\gtrsim 1$ PeV) and especially for UHE neutrino experiments based on the "Space-Airwatch" method.

Indeed, extraterrestrial ν_τs will produce detectable upgoing showers from the whole lower semisphere, whereas showers produced by UHE ν_es and ν_μs can be detected from outer space only within a narrow solid angle around the horizontal directions.

Mathematically, inclusion of the processes that change the neutrino flavor and of neutrino energy loss through creation and decay of short-lived particles leads to a system of TE that *explicitly* include the density distribution along the neutrino beam path.

Figure 12 [from S. Bottai and S. Giurgola, Astropart. Phys. **18** (2003) 539 (astro-ph/0205325)]:

τ's created in CC ν_τ interactions inside the Earth could emerge from the Earth surface and eventually decay in the atmosphere. These events could be detected by EAS detectors as upwardgoing showers.

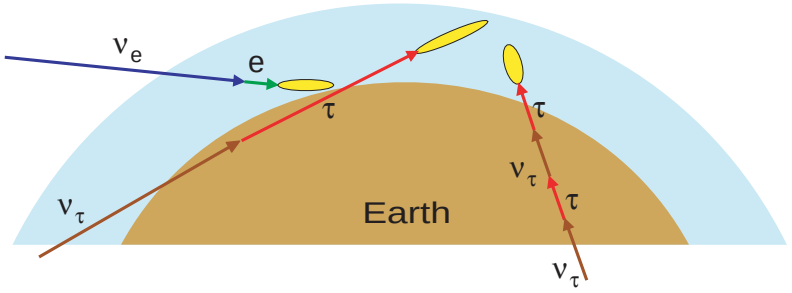

Figure 12: Schematic ν initiated air showers.

Figure 13 [from D. Fargion, astro-ph/0307485]:

Upward and horizontal τ air showers originate from UHE ν_τ's skimming the Earth. The open fan-like jets are due to geomagnetic bending at high quota ($20 - 30$ km for upward and $23 - 40$ km for horizontal showers). The shower may be pointing to an orbiting satellite detector (e.g. EUSO). The shower tail may be spread by the geomagnetic field into a thin beam observable by the detector as a small blazing oval (few dot-pixels) aligned orthogonal to the local geomagnetic field.

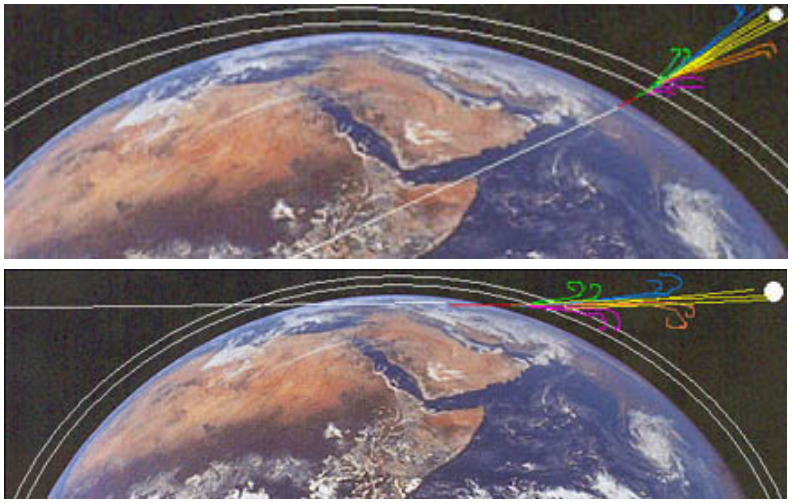

Figure 13: Upward and horizontal τ showers.

Transport equations

The generic 3D nonstationary TE for the case of chemically homogeneous matter with no external fields can be written as

$$\left[v^{-1}\partial_t + \mathbf{\Omega}\nabla + \Sigma_i(\mathbf{p},\mathbf{r})\right] F_i(\mathbf{p},\mathbf{r},t) = \sum_j \int d\Gamma_0 \Sigma^{\mathsf{s}}_{ij}(\mathbf{p}_0,\mathbf{p},\mathbf{r}) F_j(\mathbf{p}_0,\mathbf{r},t) + S_i(\mathbf{p},\mathbf{r},t).$$

Here i is the *multiindex* which marks the particle type and helicity and thus $F_i(\mathbf{p},\mathbf{r},t)$ is the flux of particles with the *definite helicity*; $d\Gamma_0 = dE_0 d\Omega_0$; the attenuation function $\Sigma_i(\mathbf{p},\mathbf{r})$ includes contributions from both absorption and decay,

$$\Sigma_i(\mathbf{p},\mathbf{r}) = \Sigma_i^{\mathsf{tot}}(E,\mathbf{r}) + \frac{m_i}{p\tau_i} = \Sigma_i^{\mathsf{tot}}(E,\mathbf{r}) + \frac{\sqrt{1-v^2}}{v\tau_i},$$

while possible contributions from decay of particles of other types are included into the source function $S_i(\mathbf{p},\mathbf{r},t)$ [defined in the whole phase space $\mathbb{R}_\mathbf{r} \otimes \mathbb{R}_\mathbf{p}$ for $0 \le t < t_1$]. The kinematic restrictions are supposed to be included into the differential macroscopic cross section $\Sigma^{\mathsf{s}}_i(\mathbf{p}_0,\mathbf{p},\mathbf{r})$ which is in fact an element of the *polarization density matrix* for corresponding process.

Note that for essentially relativistic energies, when one can neglect the bonding strengths, Fermi momenta, etc., the condition $|\mathbf{p}_0| \ge |\mathbf{p}|$ is fulfilled.

Z factor method for homogeneous TE with a smooth initial spectrum

Let us consider the simplest example, the single 1D TE

$$\left[\frac{\partial}{\partial h}+\frac{1}{\lambda(E)}\right]F(E,h)=\frac{1}{\lambda(E)}\int_0^1\frac{dx}{x^2}W(x,E)F\left(\frac{E}{x},h\right). \tag{2}$$

with the boundary condition $F(E,h=0)=F_0(E)$, where $\lambda(E)$, $W(x,E)$ are now *any* functions and $F_0(E)$ is a sufficiently smooth and nonvanishing function for any finite value of energy E. Now we *define*

$$F(E,h)=F_0(E)\exp\left[-\frac{h}{\Lambda(E,h)}\right], \tag{3a}$$

$$\Lambda(E,h)=\frac{\lambda(E)}{1-Z(E,h)}. \tag{3b}$$

The effective attenuation length, $\Lambda(E,h)$ and the Z factor contain full information about the particle's kinetics. From Eqs. (2) and (3) it immediately follows that

$$0<Z(E,h)<1.$$

Substituting (2) into the TE (2), we find that the Z factor obeys the equation

$$\left(\frac{\partial}{\partial h}+\frac{1}{h}\right)Z(E,h)=\frac{1}{h}\int_0^1\eta(x,E)W(x,E)\exp\left[\frac{h}{\Lambda(E,h)}-\frac{h}{\Lambda(E/x,h)}\right]dx, \quad (4)$$

where

$$\eta(x,E)=\frac{F_0(E/x)}{x^2F_0(E)}. \quad (5)$$

The initial spectra of astrophysical interest decrease much faster than E^2. Thus

$$0<\eta(x,E)<1 \quad \text{and} \quad \eta(0,E)=0.$$

In particular, for a purely power-law boundary spectrum, $F_0(E)\propto E^{-(\gamma+1)}$, we have

$$\eta(x,E)=x^{\gamma-1}.$$

Integrating Eq. (2) by parts, we find that the Z factor obeys the integral equation

$$Z(E,h)=\frac{1}{h}\int_0^h dh'\int_0^1\eta(x,E)W(x,E)\exp\left[-h'D(x,E,h')\right]dx, \quad (6)$$

where

$$D(x,E,h)=\frac{1-Z(E/x,h)}{\lambda(E/x)}-\frac{1-Z(E,h)}{\lambda(E)}.$$

Although this equation is nonlinear, it is much more convenient to solve it by an iterative process than the original TE (2). The rate at which the iterative process

converges depends on the choice of the zero-order approximation. The simplest choice is

$$Z^{(0)}(E,h) = 0$$

in which case

$$D^{(0)}(x,E,h) \equiv \mathcal{D}(x,E) = \frac{1}{\lambda(E/x)} - \frac{1}{\lambda(E)} \tag{7}$$

is independent of h and, in the first approximation, we have

$$Z^{(1)}(E,h) = \int_0^1 \eta(x,E) W(x,E) \left\{ \frac{1-\exp\left[-h\mathcal{D}(x,E)\right]}{h\mathcal{D}(x,E)} \right\} dx. \tag{8}$$

Small depths. Considering that, in the integrand on the right-hand side of Eq. (8), the small-x region is cut off by the $\eta(x,E)$, we can formally expand the braced expression in powers of h. This yields

$$Z^{(1)}(E,h) = \int_0^1 \eta(x,E) W(x,E) \left[1 - \frac{1}{2} h\mathcal{D}(x,E) + \ldots \right] dx. \tag{9}$$

The leading term of the expansion in Eq. (9) is

$$Z(E,0) = \int_0^1 \eta(x,E) W(x,E) dx$$

Large depths. Taking into account the known growth of $\sigma^{\text{in}}_{pA}(E)$ with energy and using Eqs. (7) and (9), we can easily show that

$$\lim_{h\to\infty} Z^{(0)}(E,h) = 0.$$

Under quite general assumptions, it can also be proven that

$$\lim_{h\to\infty} Z(E,h) = 0.$$

Therefore, the effective attenuation length $\Lambda(E,h)$ coincides with the interaction length, $\lambda(E)$ at sufficiently large depths. We will not present here the proof of this statement because it is of purely academic interest for the several reasons (disregard of 3D effects, of energy losses, and of the contribution of nucleons from mesonnucleus interactions).

What only counts is that, with increasing depth, Z decreases, which means that the relative contribution of regeneration processes is reduced. As a consequence, the energy spectrum becomes steeper with increasing depth.

Thus, even the first-approximation expression (8) for the Z factor has a correct asymptotic behavior both at small and at large values of h.

The Earth's interior

Let us neglect the nonsphericity of the Earth. The column depth of the Earth in direction ϑ between the neutrino entrant point A and the current point B, defined parametrically by the angle α, is given by

$$h = \begin{cases} \mathfrak{h}_\oplus(\alpha,\vartheta), & \text{for } 0 \le \alpha \le \frac{\pi}{2} - \vartheta, \\ 2\mathfrak{h}_\oplus\left(\frac{\pi}{2} - \vartheta, \vartheta\right) - \mathfrak{h}_\oplus(\alpha,\vartheta), & \\ \qquad \text{for } \frac{\pi}{2} - \vartheta < \alpha \le \pi - 2\vartheta, & \end{cases}$$

where

$$\mathfrak{h}_\oplus(\alpha,\vartheta) = \int_{R(\alpha,\vartheta)}^{R_\oplus} \frac{\rho(R)dR}{\sqrt{1 - \sin^2\vartheta\left(\frac{R_\oplus}{R}\right)^2}},$$

$$R(\alpha,\vartheta) = \frac{R_\oplus \sin\vartheta}{\sin(\alpha+\vartheta)},$$

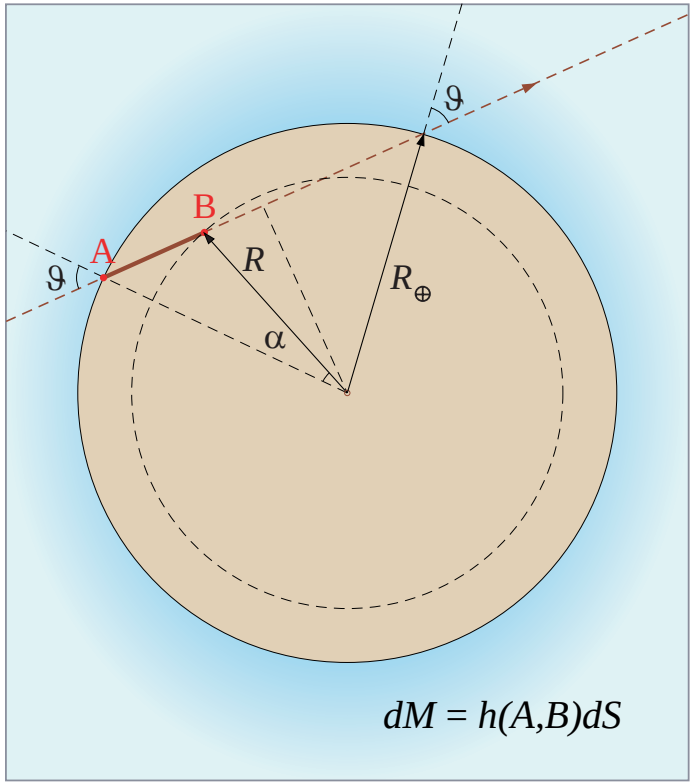

Figure 14: Definition of variables to derive the column depth, $h = h(\alpha,\vartheta)$, for the Earth.

$\rho(R)$ is the radial density distribution and $R_\oplus = 6378.14\,\text{km}$ is the (mean) radius of the Earth.

The column depth of the Earth along the whole chord ($\alpha = \pi - 2\vartheta$) is given by

$$h_\vartheta = 2\mathfrak{h}_\oplus\left(\frac{\pi}{2} - \vartheta, \vartheta\right) = 2\int_{R_\oplus \sin\vartheta}^{R_\oplus} \rho(R)\left[1 - \sin^2\vartheta\left(\frac{R_\oplus}{R}\right)^2\right]^{-1/2} dR.$$

"Almost everything known or inferred about the inner core, from seismology or indirect inference, is controversial." (Don Anderson)

The volumetric relation of the various regions of the core to the whole Earth is shown: outer core (pale blue) occupies 15%, the inner core (pink) occupies less than 1%, and the innermost inner core (red) constitutes only 0.01% of the Earth's volume. The Earth's core lies beneath 3,000-km thick, heterogeneous mantle (anomalies with higher than average seismic speed are shown in blue and those with lower than average speed are shown in red), making investigations of core properties challenging.

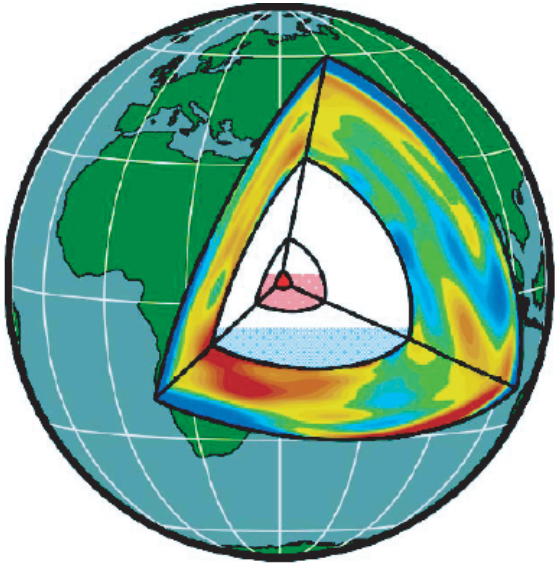

Figure 15: The Earth's interior. [From D. L. Anderson, Proc. Natl. Acad. Sci. USA **99** (2002) 13966.]

For the radial density distribution inthe Earth, it is now conventional to use the so-called "Preliminary Reference Earth Model" (PREM).[a] In this model, the Earth is divided into 10 concentric layers and the density distribution, $\rho = \rho(R)$, in each layer is approximated by a cubical polynomial:

$$\rho(R) = \sum_{k=0}^{3} a_{nk} \left(R/R_\oplus\right)^k ,$$

$$R_n \le R < R_{n+1},$$

$$n = 0, 1, \ldots, 9$$

$$(R_0 = 0,\ R_{10} = R_\oplus).$$

The nonzero coefficients a_{nk} [in g/cm^3] are listed in Table 3. Graphical representation of the model is shown in Fig. 16.

Table 3: Coefficients of the polynomials for the PREM.

n	R_{n+1} (km)	a_{n0}	a_{n1}	a_{n2}	a_{n3}
0	1221.5	13.0885		-8.8381	
1	3480.0	12.5815	-1.2638	-3.6426	-5.5281
2	5701.0	7.9565	-6.4761	5.5283	-3.0807
3	5771.0	5.3197	-1.4836		
4	5971.0	11.2494	-8.0298		
5	6151.0	7.1089	-3.8045		
6	6346.6	2.6910	0.6924		
7	6356.0	2.9000	← *crust* (must be replaced		
8	6368.0	2.6000	with the local values)		
9	6371.0	1.0200	← *ocean* (ditto)		

[a] A. M. Dziewonski and D. L. Anderson, Phys. Earth Planet. Inter. **25** (1981) 297; see also A. M. Dziewonski, "Earth structure, global", in Encyclopedia of solid Earth geophysics, Edited by D.E. James (Van Nostrand Reinhold, New York. 1989), p. 331.

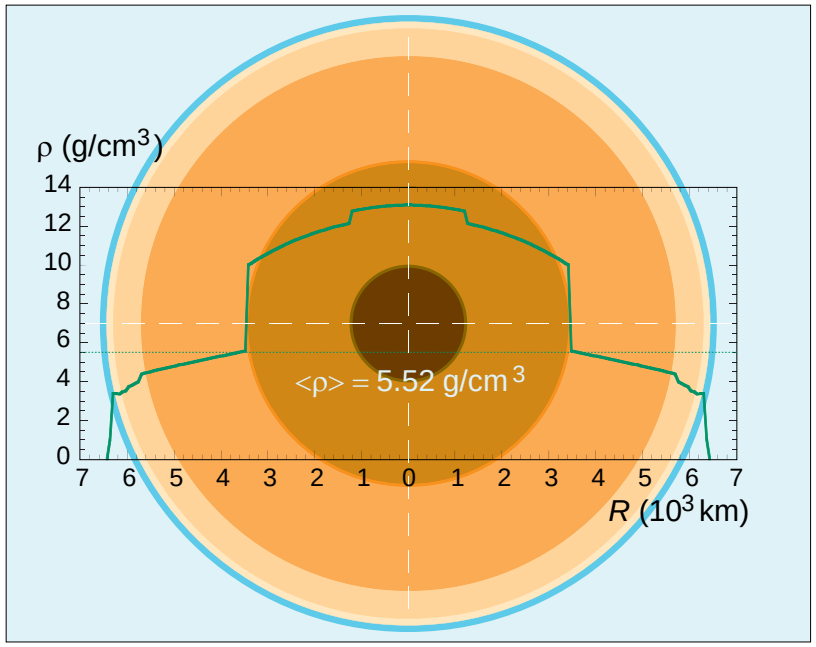

Figure 16: Radial density distribution in the Earth according to PREM.

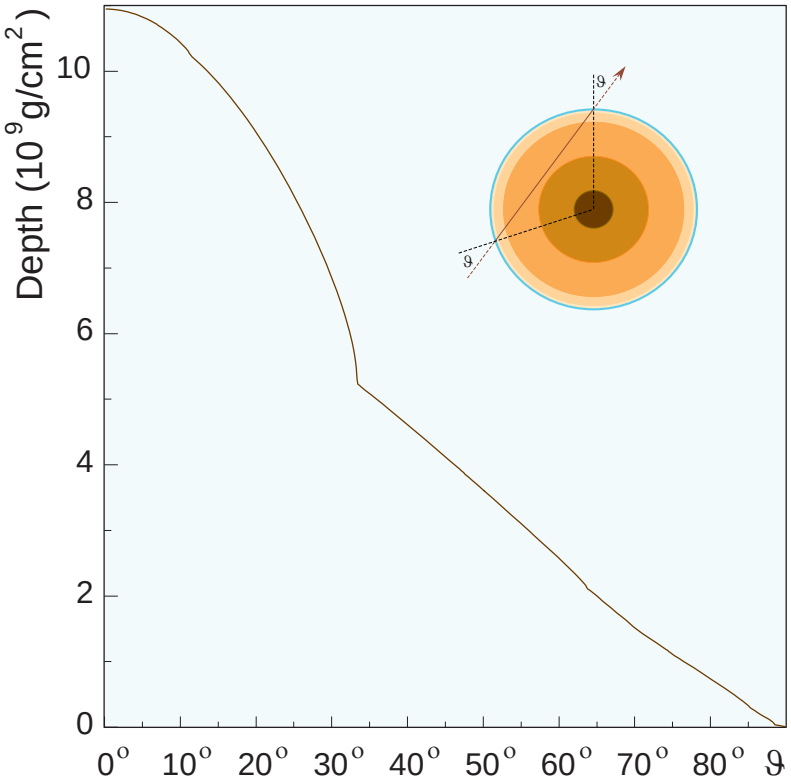

Figure 17: The column depth of the Earth (that is the depth along the total chord with the target distance of $R_\oplus \sin\vartheta$ from the center of the Earth) vs zenith angle ϑ, evaluated with the PREM.

In particular, according to PREM, the depth of Earth along the diameter is

$$h_\oplus = 2\mathfrak{h}_\oplus\,(\pi/2, 0) \simeq 1.095 \times 10^{10}\ \text{g/cm}^2.$$

$\rightarrow$

Chemical composition of the Earth

Measurements of the propagation of seismological waves in the Earths interior and studies of the properties of minerals under high pressure, have been combined to determine the chemical composition of the Earths interior.

Table 4: Masses ($\times 10^{27}$ g) of the six most abundant elements in the whole Earth's core as estimated by Herndon [J. M. Herndon, Phys. Earth Planet. Inter. **105** (1998) 1 and references therein.]

Element	1980, 1982	1993
Magnesium (Mg)	0.0475	0.0389
Silicon (Si)	0.0326	0.0376
Calcium (Ca)	0.0184	0.0178
Sulfur (S)	0.284	0.285
Iron (Fe)	1.45	1.46
Nickel (Ni)	0.0831	0.0871

The core is nearly iron.

Isotopic composition of the Earth

The mean charge-to-mass ratio, $\langle Z/A \rangle$, has been estimated by Bahcall and Krastev
[J. N. Bahcall and P. I. Krastev, Phys. Rev. C **56** (1997) 2839. The estimations are based on the experimental data from Y. Zhao and D. L. Anderson, Phys. Earth Planet. Inter. **85** (1994) 273.]

Summary:

- $\langle Z/A \rangle = 0.468$ for the core (83% Fe, 9% Ni and 8% light elements with $Z/A = 0.5$),
- $\langle Z/A \rangle = 0.497$ for the mantle (41.2% SiO_2, 52.7% MgO and 6.1% FeO).

This result is shown in Fig. 18 in terms of the number densities of u and d quarks and electrons.

$\Downarrow$

The composition is almost isoscalar.

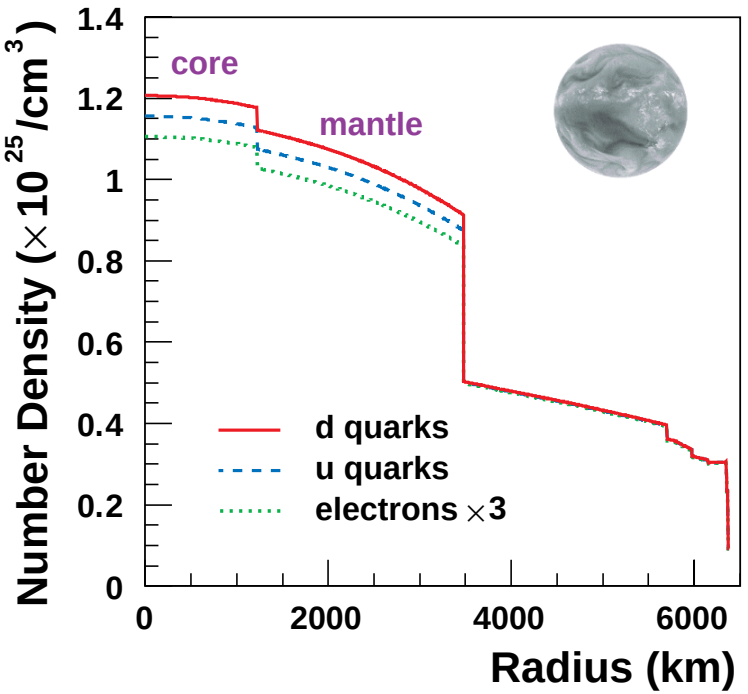

Figure 18: Estimated number densities of quarks and electrons vs distance from the center of the Earth.
[From J. Kameda, Ph. D Thesis, University of Tokyo, September, 2002.]

Numerical results for muon neutrinos

Figure 19 shows the energy dependence of the Z factors, $Z_{\nu_\mu}(E,h)$ and $Z_{\overline{\nu}_\mu}(E,h)$ for various depths, calculated with the following model for the initial neutrino spectrum:

$$F_\nu^0(E) = K\left(\frac{E_0}{E}\right)^{\gamma+1}\left(1+\frac{E}{E_0}\right)^{-\alpha}\phi\left(\frac{E}{E_{\text{cut}}}\right), \tag{10}$$

where K, γ, α, E_0, and E_{cut} are parameters and $\phi(x)$ is a function equal to 0 at $t \geq 1$ and 1 at $x \ll 1$. Varying the parameters in Eq. (10), one can approximate many models for the neutrino fluxes expected from the known astrophysical sources. Technically, the function $\phi(t)$ serves to avoid an extrapolation of the cross sections to the extremely-high energy region for which our knowledge of the parton density functions becomes doubtful. For realistic values of the parameters γ, α, and E_0, the explicit form of $\phi(t)$ is of no importance for as long as one is interested in the energy range $E \ll E_{\text{cut}}$. Here it is adopted $\phi(x) = 1/\left[1+\tan\left(\pi x/2\right)\right]$ $(x<1)$ and $E_{\text{cut}} = 3\times 10^{10}$ GeV.

The calculations were made in the fourth order of the iteration procedure. For all the spectra under discussion, for 10 GeV $\leq E \leq 10^{10}$ GeV and $0 \leq h \leq h_\oplus$, the maximum difference between $Z_\nu^{(1)}(E,h)$ and $Z_\nu^{(2)}(E,h)$ is about 4%; the value $\left|Z_\nu^{(3)}/Z_\nu^{(2)}-1\right|$ is less than 2×10^{-3}, and $\left|Z_\nu^{(4)}/Z_\nu^{(3)}-1\right|$ is less than the precision of the numerical integration and interpolation (about 10^{-5}) adopted in the calculations.

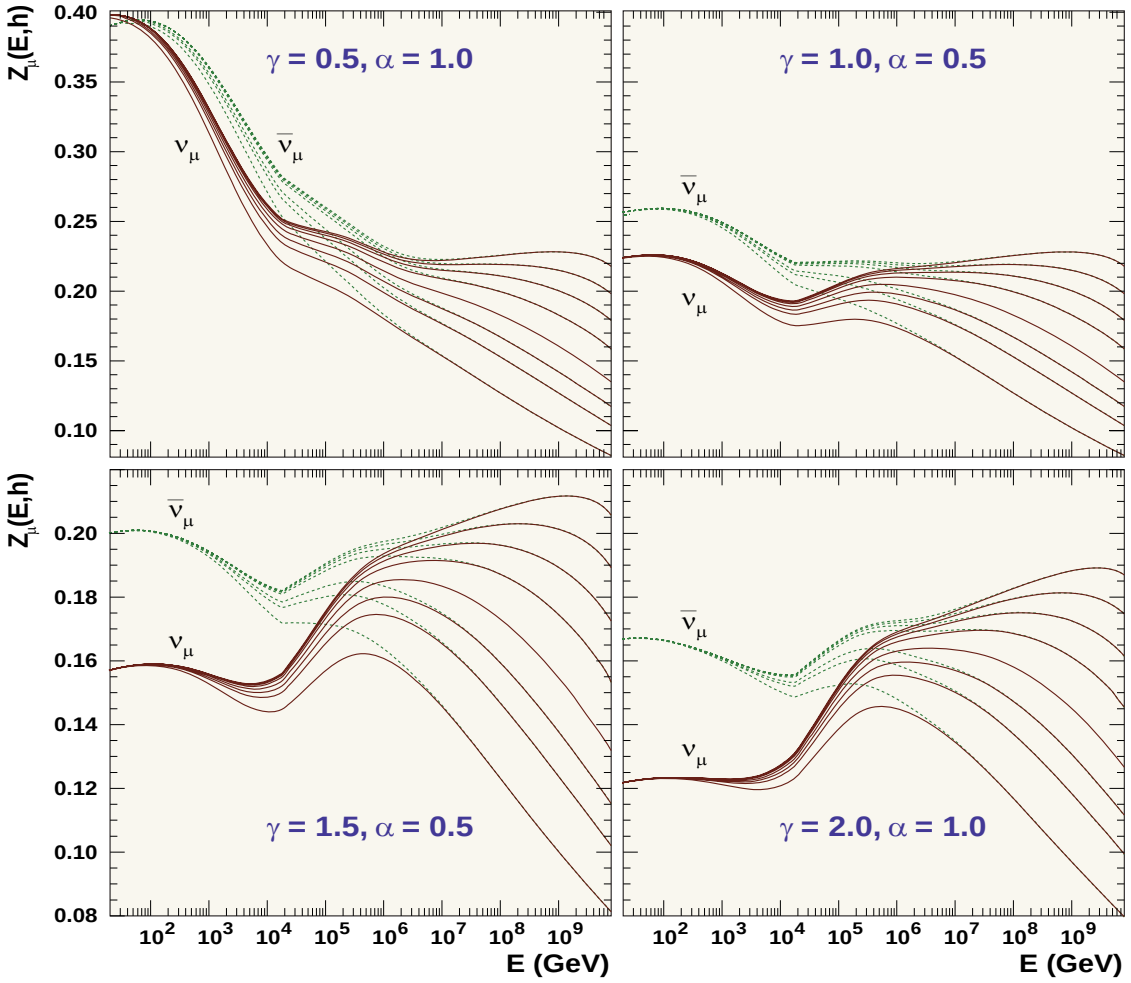

Figure 19: Z factors, $Z_{\overline{\nu}_\mu}(E,h)$ and $Z_{\nu_\mu}(E,h)$ vs energy calculated with four different sets of γ's and α's (everywhere $E_0 = 1$ PeV) for depths $h = h_\oplus/k$ [$k = 1, 2, 3, 5, 10, 20, 50$ from bottom to top] and $h = 0$ (the largest Z factors).

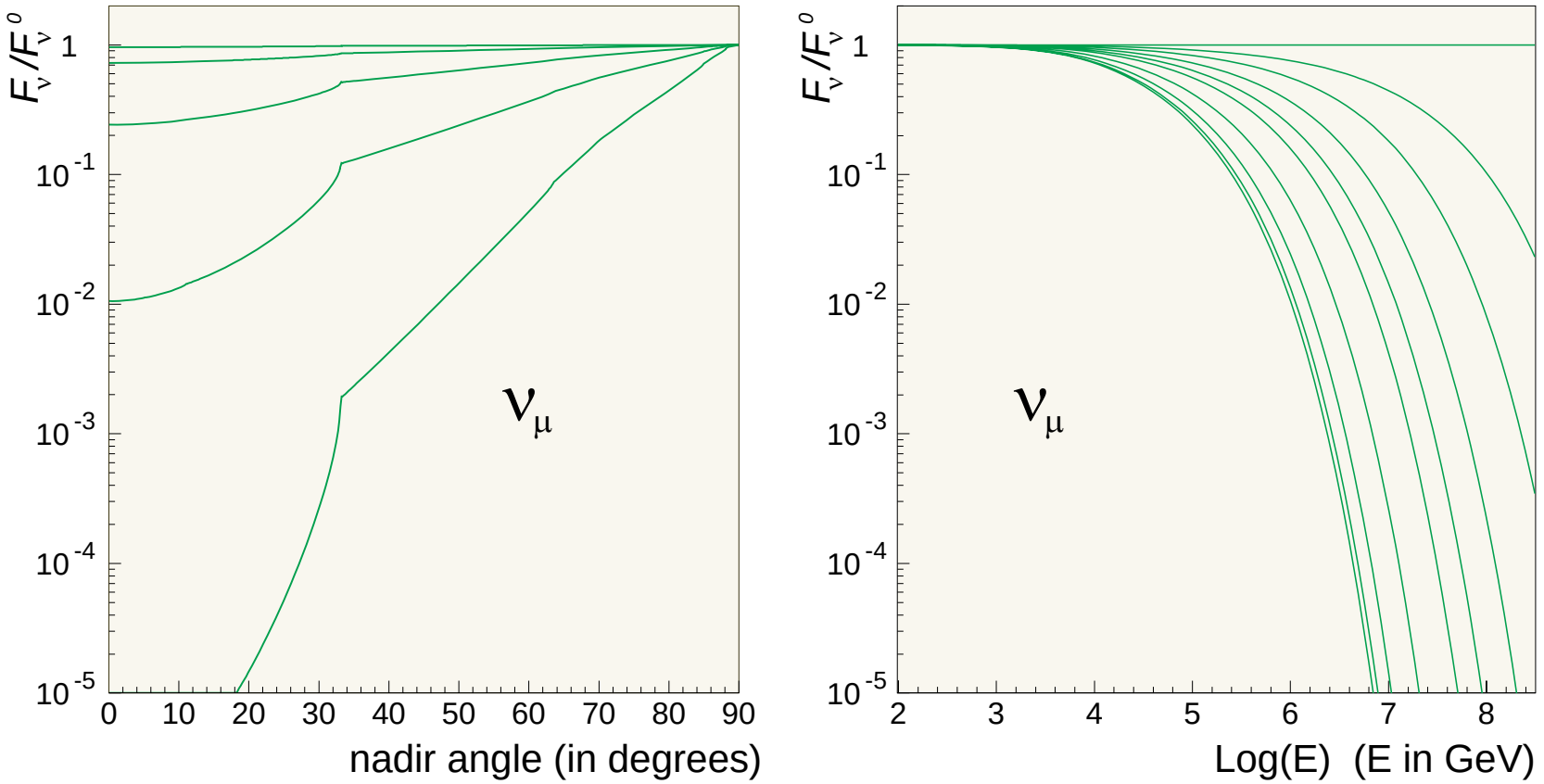

Figure 20: Penetration coefficients, $P = F_\nu/F_\nu^0 = \exp\left[-h/\Lambda_\nu(E,h)\right]$, in the Earth for for muon neutrinos with the quasi-power-law initial spectrum ($\gamma = 0.7$).
Left panel: P as a function of nadir angle ($= \pi - \vartheta$) for $E = 10^k$ GeV [$k = 3, 4, \ldots, 7$ from top to bottom]. The kinks are due to the layered structure of the Earth.
Right panel: P as a function of E at fixed nadir angles [$0^\circ, 10^\circ, \ldots, 90^\circ$ from bottom to top].

Some highlights

- As is clear from Fig. 19, the shape of the Z factors is very dependent from the initial neutrino spectrum. This is a positive fact for neutrino astronomy, since it gives, at least in principle, the possibility to reconstruct the initial neutrino spectrum from the measured energy spectrum and angular distribution of neutrino induced muon events in a neutrino telescope.
- At comparatively low energies (except for unrealistically hard spectra like the one used in Fig. 19.a), the Z factors for antineutrinos exceed those for neutrinos. Considering the inequality

  $$\lambda^{\mathsf{in}}_{\overline{\nu}_\mu}(E) > \lambda^{\mathsf{in}}_{\nu_\mu}(E),$$

  one can conclude that

  $$\Lambda_{\overline{\nu}_\mu}(E,h) > \Lambda_{\nu_\mu}(E,h)$$

  for any depth. In the multi-PeV energy range and above, the Z factors (and effective attenuation lengths) are identical for ν_μ and $\overline{\nu}_\mu$. The difference between the shapes of $Z_{\nu_\mu}(E,h)$ and $Z_{\overline{\nu}_\mu}(E,h)$ is almost depth-independent and becomes more important for steep initial spectra.

  This behavior may be understood from an analysis of the shapes of the total cross sections and regeneration functions for ν_μ and $\overline{\nu}_\mu$.

- At any fixed energy, the Z factors monotonically decrease with increasing depth and the inequality $Z_\nu(E,h) < Z^0_\nu(E)$ takes place for any $h > 0$. This effect leads to a significant decrease of the neutrino event rates in comparison with those estimated in the approximation

  $$Z_\nu \approx Z^0_\nu;$$

  the latter only works at low energies, when the shadow effect is by itself small (that is when the medium is almost transparent for neutrinos). Although these conclusions were derived from particular models for the initial neutrino spectrum, cross sections, and medium, they are actually highly general and model-independent.

  Moreover, similar effects take place in many problems of high-energy particle transport (nuclear cascade in the atmosphere, muon propagation through dense media, etc.).

- After tests with many models for the initial spectrum, we can conclude that the convergence of the algorithm is very good and that even the first approximation, $Z^{(1)}_\nu(E,h)$, has an accuracy quite sufficient for the majority of applications of the theory.

Atmospheric neutrino attenuation in the Earth

Figures 21–24 show different characteristics of the muon atmospheric (anti)neutrino propagation through the Earth calculated in the first approximation of the Z factor method. They seem to be selfexplanatory.

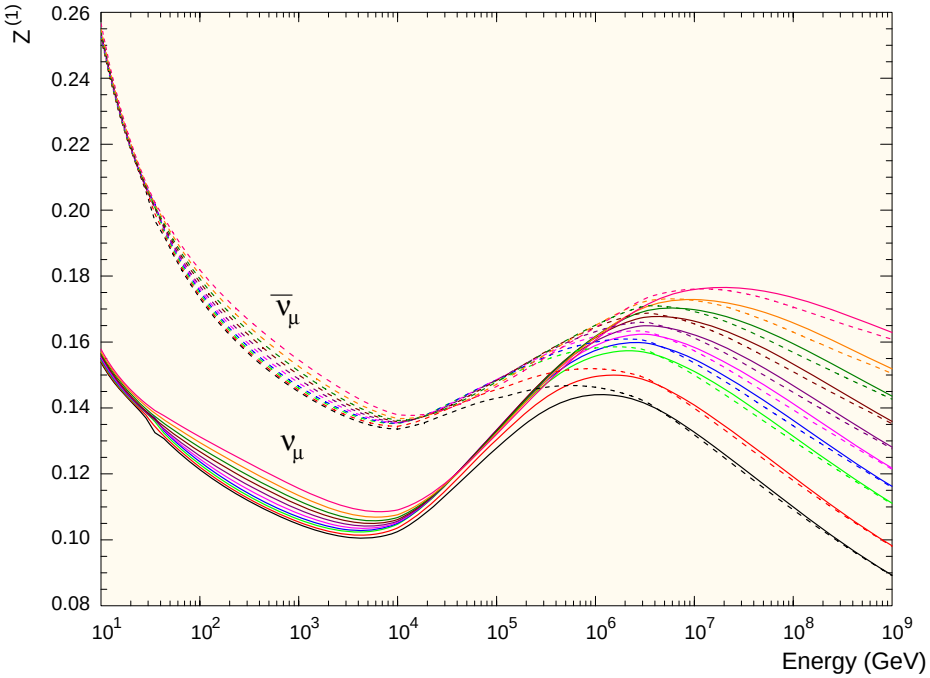

Figure 21: Z factors for atmospheric ν_μ (solid curves) and $\overline{\nu}_\mu$ (dashed curves) vs energy, calculated in the 1st approximation in for $\cos\vartheta = -0.1,\ -0.2, \ldots, -1.0$ (the sequence corresponds to the curves from top to bottom).

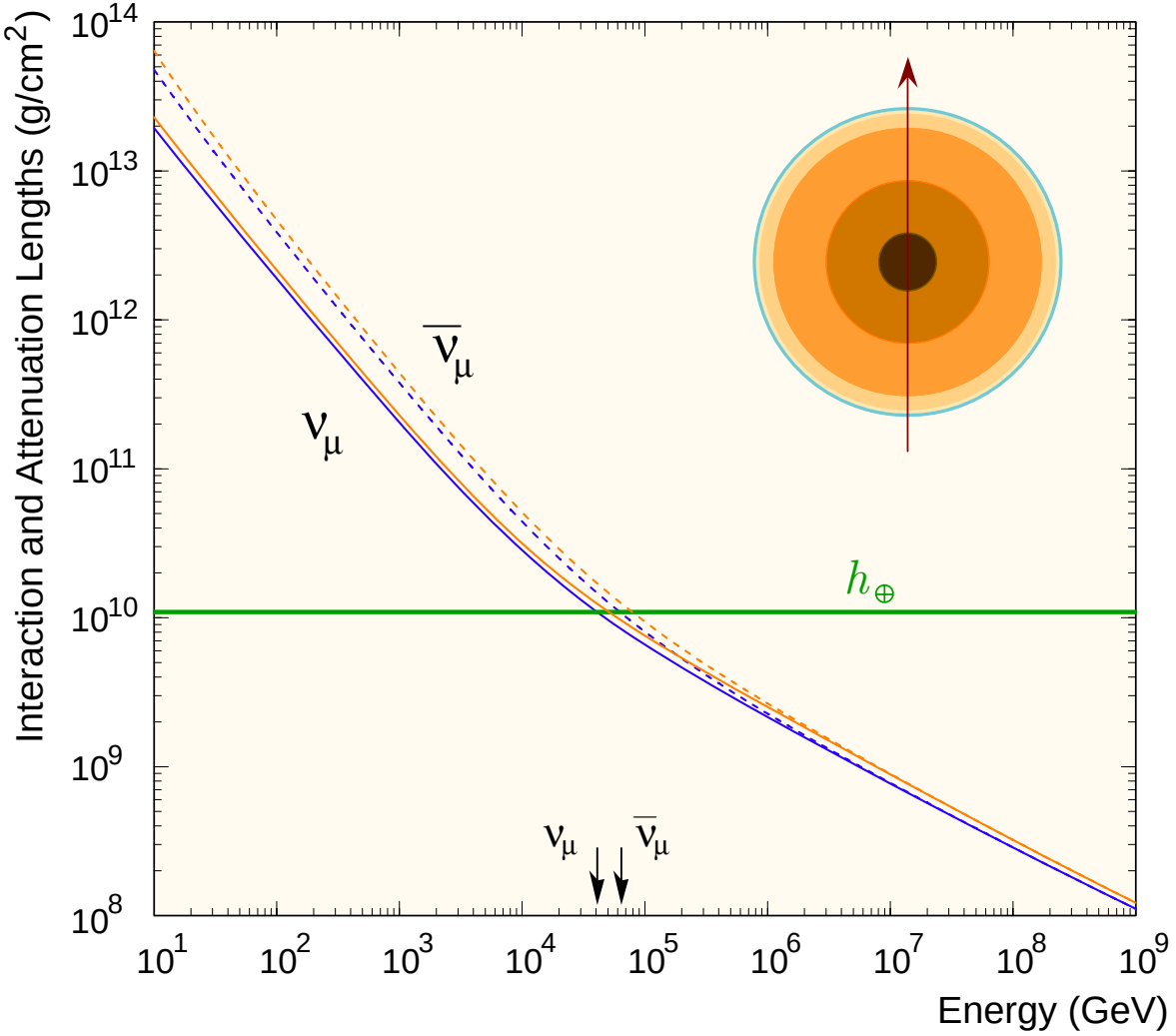

Figure 22: Interaction and attenuation lengths for atmospheric upwardgoing ν_μ and $\overline{\nu}_\mu$ in the Earth. The total depth of the Earth along its diameter is also shown for comparison.

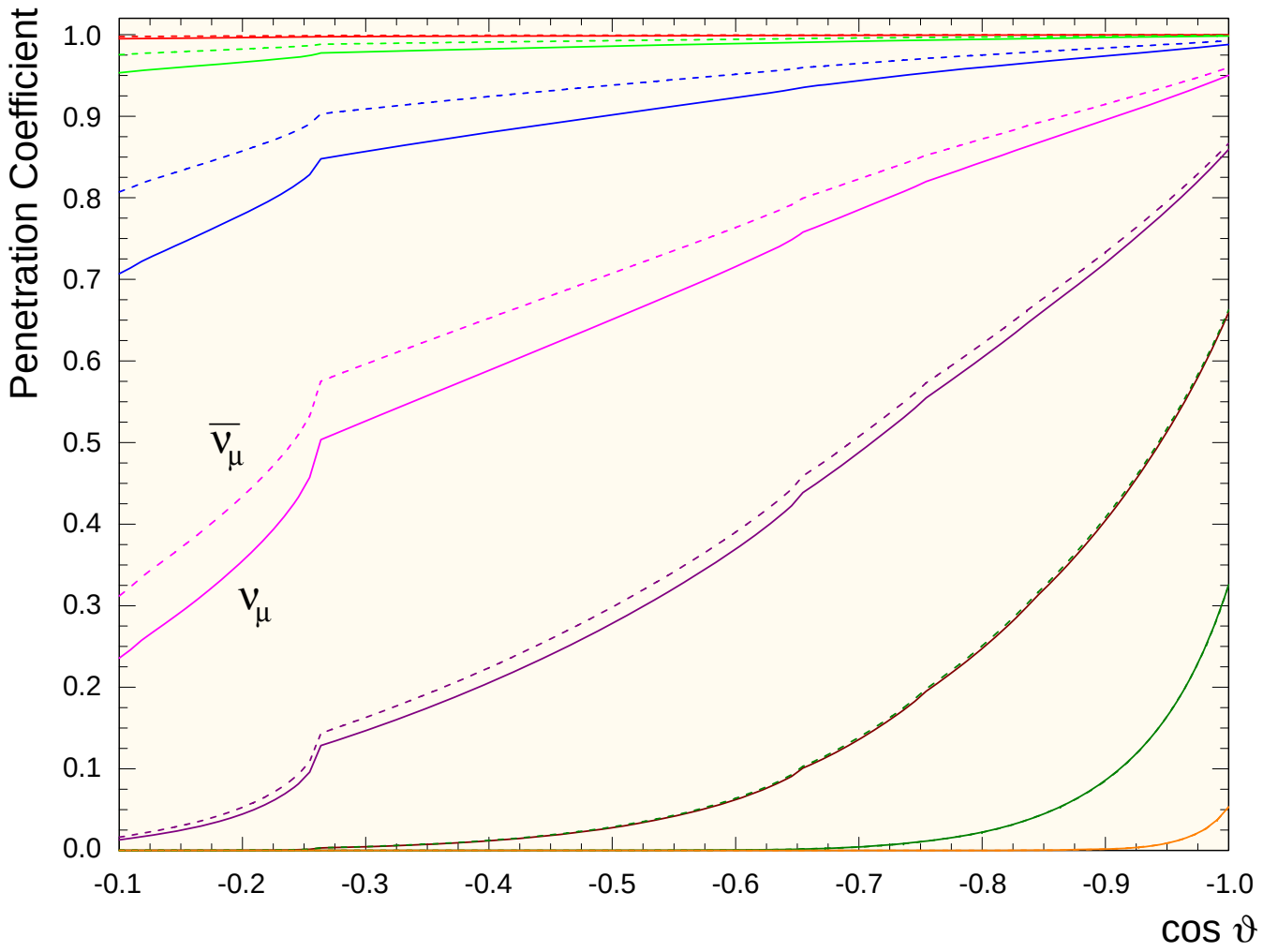

Figure 23: Penetration coefficients for atmospheric ν_μ (solid curves) and $\overline{\nu}_\mu$ (dashed curves) vs $\cos\vartheta$ for energies $E_\nu = 10^k$ GeV with $k = 3, 4, \ldots, 10$ from top to bottom.

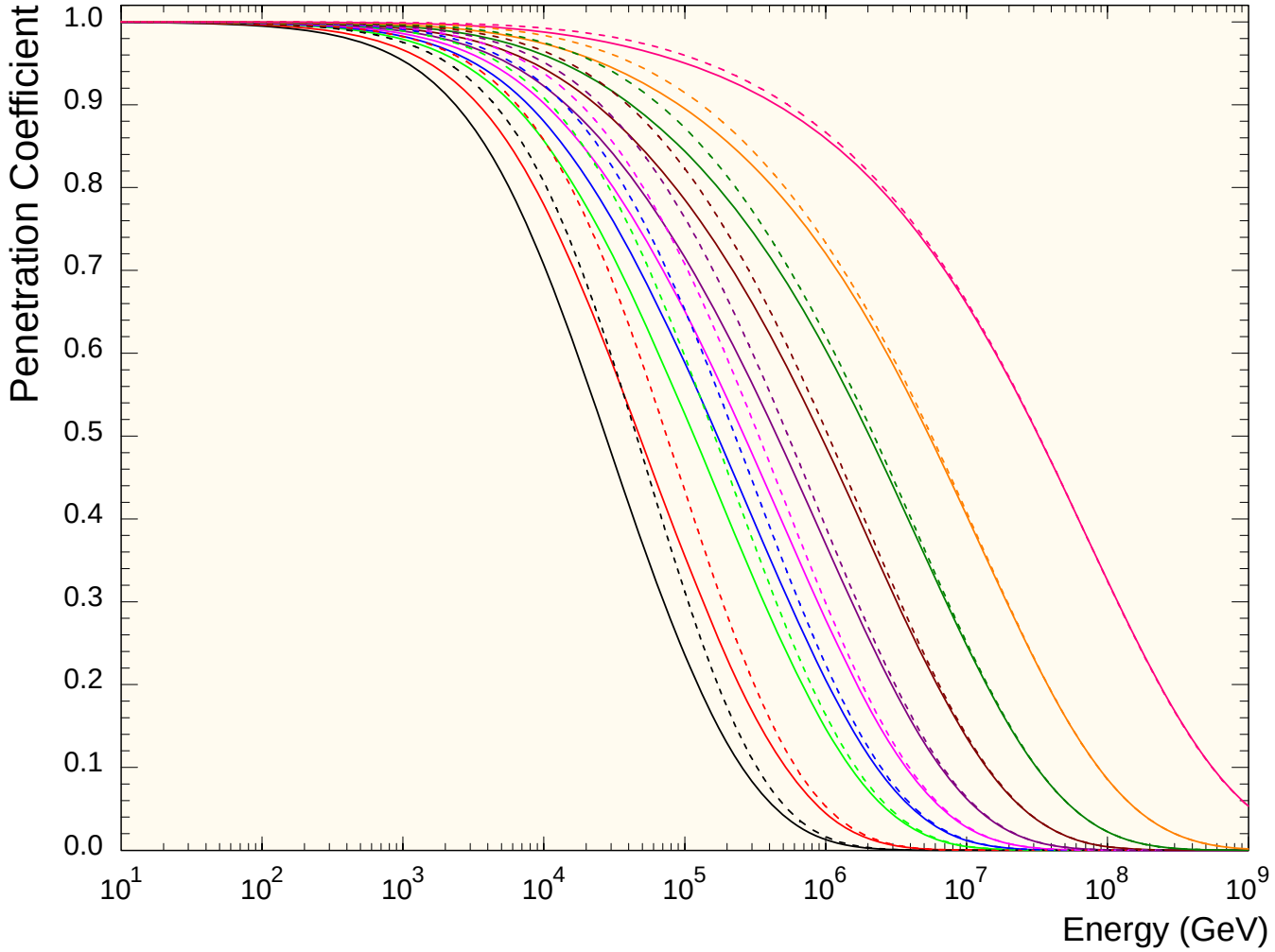

Figure 24: Penetration coefficients for atmospheric ν_μ (solid curves) and $\overline{\nu}_\mu$ (dashed curves) vs energy for $\cos\vartheta = -0.1,\ -0.2, \ldots, -1.0.$ (from top to bottom).

High-energy neutrino oscillations in matter

Neutrino refraction

It has been noted by Wolfenstein[a] that neutrino oscillations in a medium are affected by interactions even if the thickness of the medium is negligible in comparison with the neutrino mean free path.

Let us forget for the moment about the inelastic collisions and consider the simplest case of a ultrarelativistic neutrino which moves in an external (effective) potential W formed by the matter background. If the neutrino momentum in vacuum was $\mathbf{p}$ then its energy was $\simeq p = |\mathbf{p}|$. When the neutrino enters into the medium, its energy becomes $E = p + W$. Let us now introduce the index of refraction $n = p/E$ which is a positive value in the absence of inelastic collisions. Therefore

$$W = (1 - n)E \simeq (1 - n)p. \tag{11}$$

In the last step, we took into account that neutrino interaction with matter is very weak, $|W| \ll E$, and thus $E \simeq p$ is a good approximation.

The time evolution equation for the neutrino flavor states in matter follows from a simple consideration and the quantum-mechanical correspondence principle.

[a] L. Wolfenstein, Phys. Rev. D **17** (1978) 2369.

This is the famous Wolfenstein equation:

$$i\frac{d}{dt}|\nu(t)\rangle_{\mathsf{f}} = \left[\mathbf{V}\mathbf{H}_0\mathbf{V}^\dagger + \mathbf{W}(t)\right]|\nu(t)\rangle_{\mathsf{f}}, \tag{12}$$

where

$$\mathbf{W}(t) = \mathsf{diag}\left(1 - n_{\nu_e}, 1 - n_{\nu_\mu}, 1 - n_{\nu_\tau}, \ldots\right) p \tag{13}$$

is the interaction Hamiltonian.

It will be useful for the following to introduce the *time-evolution operator* for the flavor states defined by

$$|\nu(t)\rangle_{\mathsf{f}} = \mathbf{S}(t)|\nu(0)\rangle_{\mathsf{f}}.$$

Taking into account that $|\nu(t)\rangle_{\mathsf{f}}$ must satisfy Eq. (12) for any initial condition $|\nu(t=0)\rangle_{\mathsf{f}} = |\nu(0)\rangle_{\mathsf{f}}$, the Wolfenstein equation can be immediately rewritten in terms of the evolution operator:

$$i\dot{\mathbf{S}}(t) = \left[\mathbf{V}\mathbf{H}_0\mathbf{V}^\dagger + \mathbf{W}(t)\right]\mathbf{S}(t), \quad \mathbf{S}(0) = \mathbf{1}. \tag{14}$$

This equation (or its equivalent (12)) cannot be solved analytically in the general case of a medium with a varying (along the neutrino pass) density. But for a medium with a slowly (adiabatically) varying density distribution the approximate solution can be obtained by a diagonalization of the effective Hamiltonian. Below we will consider this method for a rather general 2-flavor case but now let us illustrate (without derivation) the simplest situation with a matter of constant density.

Matter of constant density

In the 2-flavor case, the transition probability is given by the formula very similar to that for vacuum:

$$P_{\alpha\alpha'}(L) = \frac{1}{2}\sin^2 2\theta_{\mathsf{m}}\left[1-\cos\left(\frac{2\pi L}{L_{\mathsf{m}}}\right)\right],$$

$$L_{\mathsf{m}} = L_{\nu}\left[1-2\kappa\left(L_{\nu}/L_0\right)\cos\theta+\left(L_{\nu}/L_0\right)^2\right]^{-1/2}.$$

The L_{m} is called the oscillation length in matter and is defined through the following quantities:

$$L_{\nu}\equiv L_{23}=\frac{4\pi E}{\Delta m^2},\quad L_0=\frac{\sqrt{2}\pi A}{G_F N_A Z\rho}\approx 2R_{\oplus}\left(\frac{A}{2Z}\right)\left(\frac{2.5\ \mathrm{g/cm}^3}{\rho}\right),$$

$$\kappa=\mathsf{sign}\left(m_3^2-m_2^2\right),\quad \Delta m^2=\left|m_3^2-m_2^2\right|.$$

The parameter θ_{m} is called the mixing angle in matter and is given by

$$\sin 2\theta_{\mathsf{m}}=\sin 2\theta\left(\frac{L_{\mathsf{m}}}{L_{\nu}}\right),\quad \cos 2\theta_{\mathsf{m}}=\left(\cos 2\theta-\kappa\frac{L_{\nu}}{L_0}\right)\left(\frac{L_{\mathsf{m}}}{L_{\nu}}\right).$$

The solution for antineutrinos is the same but with the replacement $\kappa\mapsto-\kappa$. The closeness of the value of L_0 to the Earth's diameter is even more surprising than that for L_{ν}. The matter effects are important for atmospheric neutrinos.

Propagation of high-energy mixed neutrinos through matter

"The matter doesn't matter"

Lincoln Wolfenstein, lecture given at 28th SLAC Summer Institute on Particle Physics "Neutrinos from the Lab, the Sun, and the Cosmos", Stanford, CA, Aug. 14-25, 2000.

When neutrinos propagate through vacuum there is a phase change

$$\exp\left(-im_i^2 t/2p_\nu\right).$$

For two mixed flavors there is a resulting oscillation with length

$$L_{\text{vac}} = \frac{4\pi E_\nu}{\Delta m^2} \approx D_\oplus \left(\frac{E_\nu}{10\ \text{GeV}}\right)\left(\frac{0.002\ \text{eV}^2}{\Delta m^2}\right).$$

In matter there is an additional phase change due to refraction associated with forward scattering

$$\exp\left[ip_\nu(\text{Re}\, n - 1)t\right]$$

and the characteristic length (for a normal medium) is

$$L_{\text{ref}} = \frac{\sqrt{2}A}{G_F N_A Z \rho} \approx D_\oplus \left(\frac{A}{2Z}\right)\left(\frac{2.5\ \text{g/cm}^2}{\rho}\right).$$

It is generally believed that the imaginary part of the index of refraction n which describes the neutrino absorption due to inelastic interactions *does not affect the oscillation probabilities* or at the least inelastic interactions can be someway *decoupled* from oscillations.

The conventional arguments are

- $\mathrm{Re}\, n - 1 \propto G_F$ while $\mathrm{Im}\, n \propto G_F^2$;
- Only Δn may affect the oscillations and $\Delta \mathrm{Im}\, n$ is all the more negligible.

It will be shown that these arguments do not work for sufficiently high neutrino energies and/or for thick media $\Longrightarrow$ in general absorption cannot be decoupled from refraction and mixing.

By using another cant phrase of Wolfenstein, one can say that

"In some circumstances the matter could matter."

Generalized MSW equation

Let $f_{\nu_\alpha A}(0)$ be the amplitude for the ν_α zero-angle scattering from particle A of the matter background ($A = e, p, n, \ldots$),
$\rho(t)$ – the matter density (in g/cm^3),
$Y_A(t)$ – the number of particles A per amu in the point t of the medium,
$N_0 = 6.02214199 \times 10^{23}$ cm^{-3} – the reference particle number density (numerically equal to the Avogadro's number).

Then the index of refraction of ν_α for small $|n-1|$ is given by

$$n_\alpha(t) = 1 + \frac{2\pi N_0 \rho(t)}{p_\nu^2} \sum_A Y_A(t) f_{\nu_\alpha A}(0),$$

where p_ν is the neutrino momentum. Since the amplitude $f_{\nu_\alpha A}(0)$ is in general a complex number, the index of refraction is also complex. Its real part is responsible for neutrino refraction while the imaginary part – for absorption. From the optical theorem of quantum mechanics we have

$$\mathrm{Im}\left[f_{\nu_\alpha A}(0)\right] = \frac{p_\nu}{4\pi} \sigma^{\mathrm{tot}}_{\nu_\alpha A}\left(p_\nu\right).$$

This implies that

$$p_\nu \mathrm{Im}\left[n_\alpha(t)\right] = \frac{1}{2} N_0 \rho(t) \sum_A Y_A(t) \sigma^{\mathrm{tot}}_{\nu_\alpha A}\left(p_\nu\right) = \frac{1}{2\Lambda_\alpha\left(p_\nu, t\right)},$$

where $\Lambda_\alpha\left(p_\nu, t\right)$ is the mean free path of ν_α in the point t of the medium.

Note:

The dimension of Λ_α is cm,

$$\Lambda_\alpha\left(p_\nu, t\right) = \frac{1}{\Sigma_\alpha^{\text{tot}}\left(p_\nu, t\right)} = \frac{\lambda_a^{\text{tot}}\left(p_\nu, t\right)}{\rho(t)}.$$

Since the neutrino momentum, p_ν, is an extrinsic variable in Eq. (15), we will sometimes omit this argument to simplify formulas.

The generalized MSW equation for the time-evolution operator

$$\mathbf{S}(t) = \begin{pmatrix} S_{\alpha\alpha}(t) & S_{\alpha\beta}(t) \\ S_{\beta\alpha}(t) & S_{\beta\beta}(t) \end{pmatrix}$$

of two mixed stable neutrino flavors ν_α and ν_β propagating through an absorbing medium can be written as

$$i\frac{d}{dt}\mathbf{S}(t) = \left[\mathbf{V}\mathbf{H}_0\mathbf{V}^T + \mathbf{W}(t)\right]\mathbf{S}(t), \quad (\mathbf{S}(0) = \mathbf{1})\,. \tag{15}$$

Here

$$\mathbf{V}=\begin{pmatrix}\cos\theta & \sin\theta\\ -\sin\theta & \cos\theta\end{pmatrix}$$ is the vacuum mixing matrix ($0\le\theta\le\pi/2$),

$$\mathbf{H}_0=\begin{pmatrix}E_1 & 0\\ 0 & E_2\end{pmatrix}$$ is the vacuum Hamiltonian for ν mass eigenstates,

$$E_i=\sqrt{p_\nu^2+m_i^2}\simeq p_\nu+m_i^2/2p_\nu$$ is the energy of the ν_i eigenstate,

$$\mathbf{W}(t)=-p_\nu\begin{pmatrix}n_\alpha(t)-1 & 0\\ 0 & n_\beta(t)-1\end{pmatrix}$$ is the interaction Hamiltonian.

Master equation

It is useful to transform MSW equation into the one with a traceless Hamiltonian. For this purpose we define the matrix

$$\widetilde{\mathbf{S}}(t)=\exp\left\{\frac{i}{2}\int_0^t \mathrm{Tr}\left[\mathbf{H}_0+\mathbf{W}(t')\right]dt'\right\}\mathbf{S}(t).$$

The master equation (ME) for this matrix then is

$$\boxed{i\frac{d}{dt}\widetilde{\mathbf{S}}(t)=\mathbf{H}(t)\widetilde{\mathbf{S}}(t),\quad \widetilde{\mathbf{S}}(0)=\mathbf{1}.} \qquad (16)$$

The effective Hamiltonian is defined by

$$\mathbf{H}(t) = \begin{pmatrix} q(t) - \Delta_c & \Delta_s \\ \Delta_s & -q(t) + \Delta_c \end{pmatrix},$$

$$\Delta_c = \Delta \cos 2\theta, \quad \Delta_s = \Delta \sin 2\theta, \quad \Delta = \frac{m_2^2 - m_1^2}{4p_\nu},$$

$$q(t) = q_R(t) + iq_I(t) = \frac{1}{2} p_\nu \left[n_\beta(t) - n_\alpha(t) \right].$$

The Hamiltonian for antineutrinos is of the same form as $\mathbf{H}(t)$ but

$$\mathrm{Re}\left[f_{\overline{\nu}_\alpha A}(0) \right] = -\mathrm{Re}\left[f_{\nu_\alpha A}(0) \right] \quad \text{and} \quad \mathrm{Im}\left[f_{\overline{\nu}_\alpha A}(0) \right] \neq \mathrm{Im}\left[f_{\nu_\alpha A}(0) \right].$$

The neutrino oscillation probabilities are

$$P\left[\nu_\alpha(0) \to \nu_{\alpha'}(t) \right] \equiv P_{\alpha\alpha'}(t) = \left| S_{\alpha'\alpha}(t) \right|^2 = A(t) \left| \widetilde{S}_{\alpha'\alpha}(t) \right|^2, \tag{17}$$

where

$$A(t) = \exp\left[-\int_0^t \frac{dt'}{\Lambda(t')} \right], \quad \frac{1}{\Lambda(t)} = \frac{1}{2} \left[\frac{1}{\Lambda_\alpha(t)} + \frac{1}{\Lambda_\beta(t)} \right].$$

Owing to the complex potential q, the Hamiltonian $\mathbf{H}(t)$ is non-Hermitian and the new evolution operator $\widetilde{\mathbf{S}}(t)$ is nonunitary. As a result, there are no conventional relations between $P_{\alpha\alpha'}(t)$.

Since

$$q_I(t) = \frac{1}{4}\left[\frac{1}{\Lambda_\beta(t)} - \frac{1}{\Lambda_\alpha(t)}\right],$$

the matrix $\mathbf{H}(t)$ becomes Hermitian when $\Lambda_\alpha = \Lambda_\beta$. If this is the case at any t, the ME reduces to the standard MSW equation and inelastic scattering results in the common exponential attenuation of the probabilities. probabilities. From here, we shall consider the more general and more interesting case, when $\Lambda_\alpha \neq \Lambda_\beta$.

Examples

$\nu_\alpha - \nu_s$

This is the extreme example. Since $\Lambda_s = \infty$, we have $\Lambda = 2\Lambda_\alpha$ and $q_I = -1/4\Lambda_\alpha$. So $q_I \neq 0$ at any energy. Even without solving the evolution equation, one can expect the penetrability of active neutrinos to be essentially modified in this case because, roughly speaking, they spend a certain part of life in the sterile state. In other words, sterile neutrinos "tow" their active companions through the medium as a tugboat. On the other hand, the active neutrinos "retard" the sterile ones, like a bulky barge retards its tugboat. As a result, the sterile neutrinos undergo some absorption.

$\nu_{e,\mu} - \nu_\tau$

Essentially at all energies, $\sigma^{\rm CC}_{\nu_{e,\mu}N} > \sigma^{\rm CC}_{\nu_\tau N}$. This is because of large value of the τ lepton mass, m_τ, which leads to several consequences:

1. high neutrino energy threshold for τ production;
2. sharp shrinkage of the phase spaces for CC $\nu_\tau N$ reactions;
3. kinematic correction factors ($\propto m_\tau^2$) to the nucleon structure functions (the corresponding structures are negligible for e production and small for μ production).

The neutral current contributions are canceled out from q_I. Thus, in the context of the master equation, ν_τ can be treated as (almost) sterile within the energy range for which $\sigma^{\rm CC}_{\nu_{e,\mu}N} \gg \sigma^{\rm CC}_{\nu_\tau N}$ (see Figs. 26–27 below).

$\overline{\nu}_e - \overline{\nu}_\alpha$

A similar situation, while in quite a different and narrow energy range, holds in the case of mixing of $\overline{\nu}_e$ with some other flavor. This is a particular case for a normal C asymmetric medium, because of the W boson resonance formed in the neighborhood of $E_\nu^{\rm res} = m_W^2/2m_e \approx 6.33$ PeV through the reactions

$$\overline{\nu}_e e^- \to W^- \to \text{hadrons} \quad \text{and} \quad \overline{\nu}_e e^- \to W^- \to \overline{\nu}_\ell \ell^- \quad (\ell = e, \mu, \tau).$$

Let's remind that $\sigma^{\rm tot}_{\overline{\nu}_e e} \approx 250\ \sigma^{\rm tot}_{\overline{\nu}_e N}$ just at the resonance peak (see Fig. 25 and Table 5 below).

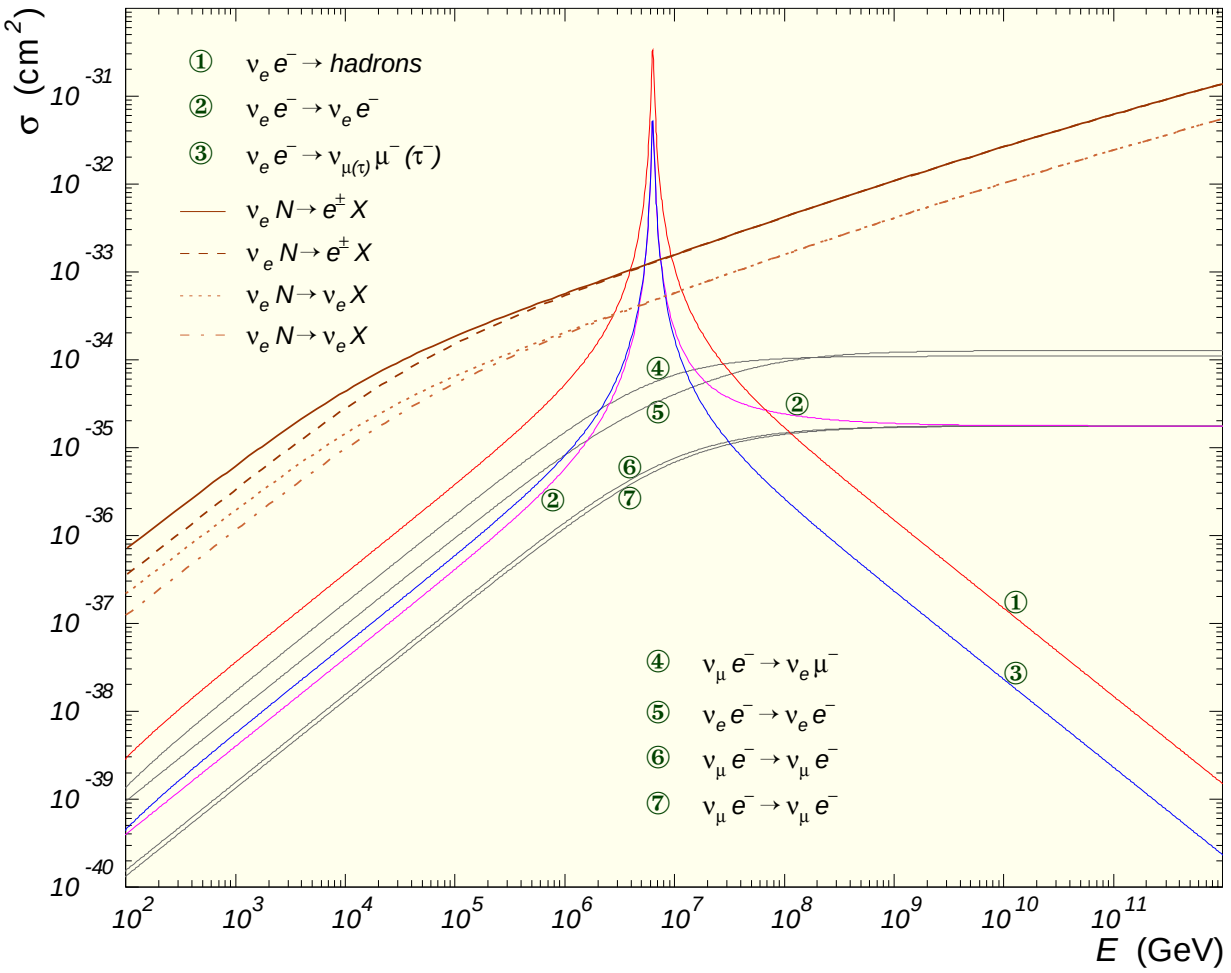

Figure 25: Total cross sections for (anti)neutrino interactions on electron targets. The cross sections for (anti)neutrino CC and NC interactions on isoscalar nucleon are also shown for a comparison.

Table 5: Integrated cross sections for neutrino-electron and neutrino-nucleon scattering at $E_\nu = m_W^2/2m_e \approx 6.331$ PeV.

Reaction	σ (cm^2)	Reaction	σ (cm^2)
$\nu_\mu e \to \nu_\mu e$	5.86×10^{-36}	$\nu_\mu N \to \mu^- +$ anything	1.43×10^{-33}
$\overline{\nu}_\mu e \to \overline{\nu}_\mu e$	5.16×10^{-36}	$\nu_\mu N \to \nu_\mu +$ anything	6.04×10^{-34}
$\nu_\mu e \to \mu \nu_e$	5.42×10^{-35}	$\overline{\nu}_\mu N \to \mu^+ +$ anything	1.41×10^{-33}
$\nu_e e \to \nu_e e$	3.10×10^{-35}	$\overline{\nu}_\mu N \to \overline{\nu}_\mu +$ anything	5.98×10^{-34}
$\overline{\nu}_e e \to \overline{\nu}_e e$	5.215×10^{-32}		
$\overline{\nu}_e e \to \overline{\nu}_\mu \mu$	5.214×10^{-32}		
$\overline{\nu}_e e \to \overline{\nu}_\tau \tau$	5.208×10^{-32}		
$\overline{\nu}_e e \to$ hadrons	3.352×10^{-31}		
$\overline{\nu}_e e \to$ anything	4.917×10^{-31}		

Just at the resonance peak, $\sigma^{\rm tot}_{\overline{\nu}_e e} \approx 250\, \sigma^{\rm tot}_{\overline{\nu}_e N}$.

Note:

The cross sections for electron targets listed in Table 5 were calculated using the formulas given by Gandhi *et al.*, [a] but some numerical values are different since the input parameters were updated.

[a] R. Gandhi, C. Quigg, M. H. Reno, and I. Sarcevic, "Ultrahigh-energy neutrino interactions," Astropart. Phys. **5** (1996) 81–110 (hep-ph/9512364).

Total cross sections

According to Albright and Jarlskog[a]

$$\frac{d\sigma^{\mathrm{CC}}_{\nu,\overline{\nu}}}{dxdy} = \frac{G_F^2 m_N E_\nu}{\pi}\left(A_1F_1 + A_2F_2 \pm A_3F_3 + A_4F_4 + A_5F_5\right),$$

where $F_i = F_i(x, Q^2)$ are the nucleon structure functions and A_i are the kinematic factors $i = 1, \ldots, 5$). These factors were calculated by many authors[b] and the most accurate formulas were given by Paschos and Yu:

$$A_1 = xy^2 + \frac{m_l^2 y}{2m_N E_\nu}, \quad A_2 = 1 - y - \frac{m_N}{2E_\nu}xy - \frac{m_l^2}{4E_\nu^2}, \quad A_3 = xy\left(1 - \frac{y}{2}\right) - \frac{m_l^2 y}{4m_N E_\nu},$$

$$A_4 = \frac{m_l^2}{2m_N E_\nu}\left(xy + \frac{m_l^2}{2m_N E_\nu}\right), \quad A_5 = -\frac{m_l^2}{2m_N E_\nu}.$$

The contributions proportional to m_ℓ^2 must vanish as $E_\nu \gg m_\ell$. However they remain surprisingly important even at very high energies.

---

[a] C. H. Albright and C. Jarlskog, Nucl. Phys. B**84** (1975) 467. See also I. Ju, Phys. Rev. D**8** (1973) 3103 and V. D. Barger *et al.*, Phys. Rev. D**16** (1977) 2141.

[b] See previous footnote and also the more recent papers: S. Dutta, R. Gandhi, and B. Mukhopadhyaya, Eur. Phys. J. C **18** (2000) 405 (hep–ph/9905475); N. I. Starkov, J. Phys. G: Nucl. Part. Phys. **27** (2001) L81; E. A. Paschos and J. Y. Yu, Phys. Rev. D**65** (2002) 033002 (hep–ph/0107261).

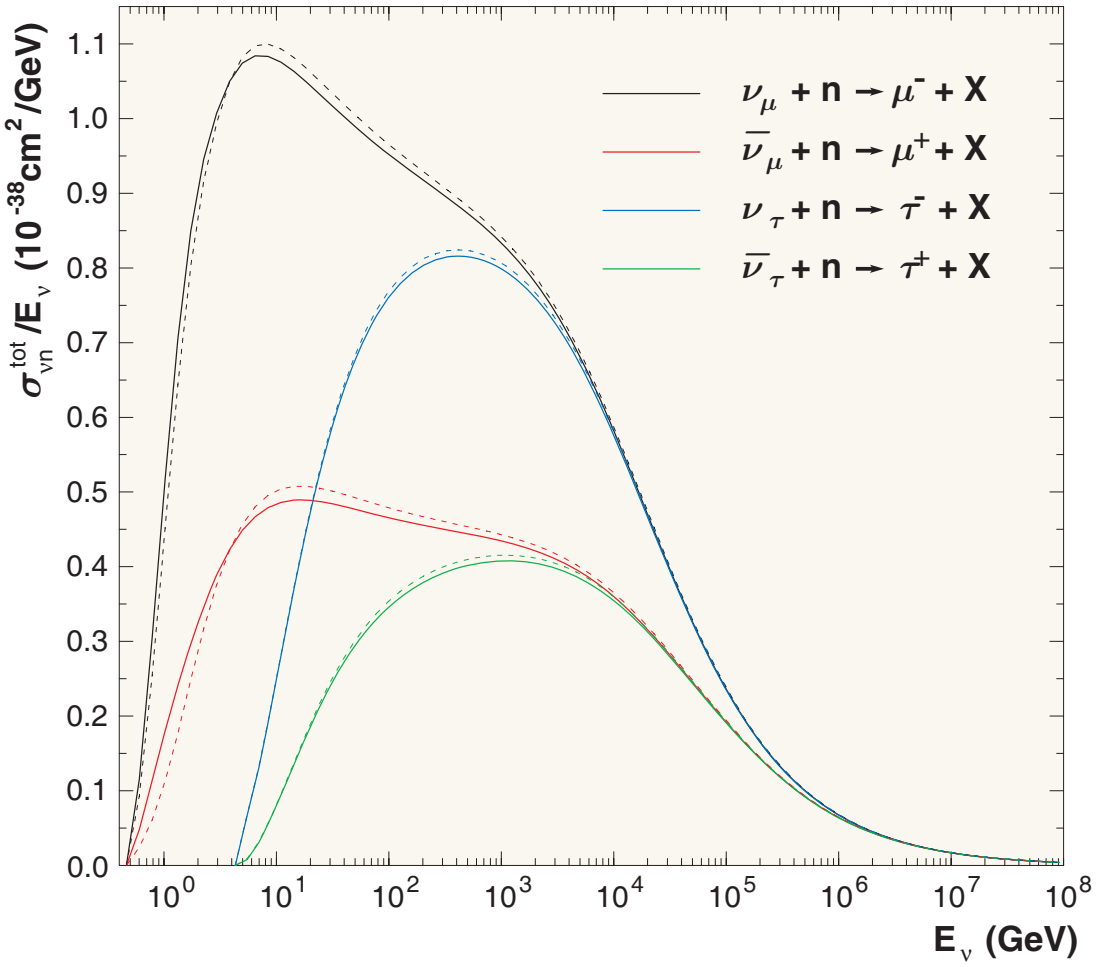

Figure 26: Total inelastic νn cross sections evaluated with the MRST 2002 NNLO PDF model modified according to Bodek–Yang prescription (solid lines) and unmodified (dashed lines).

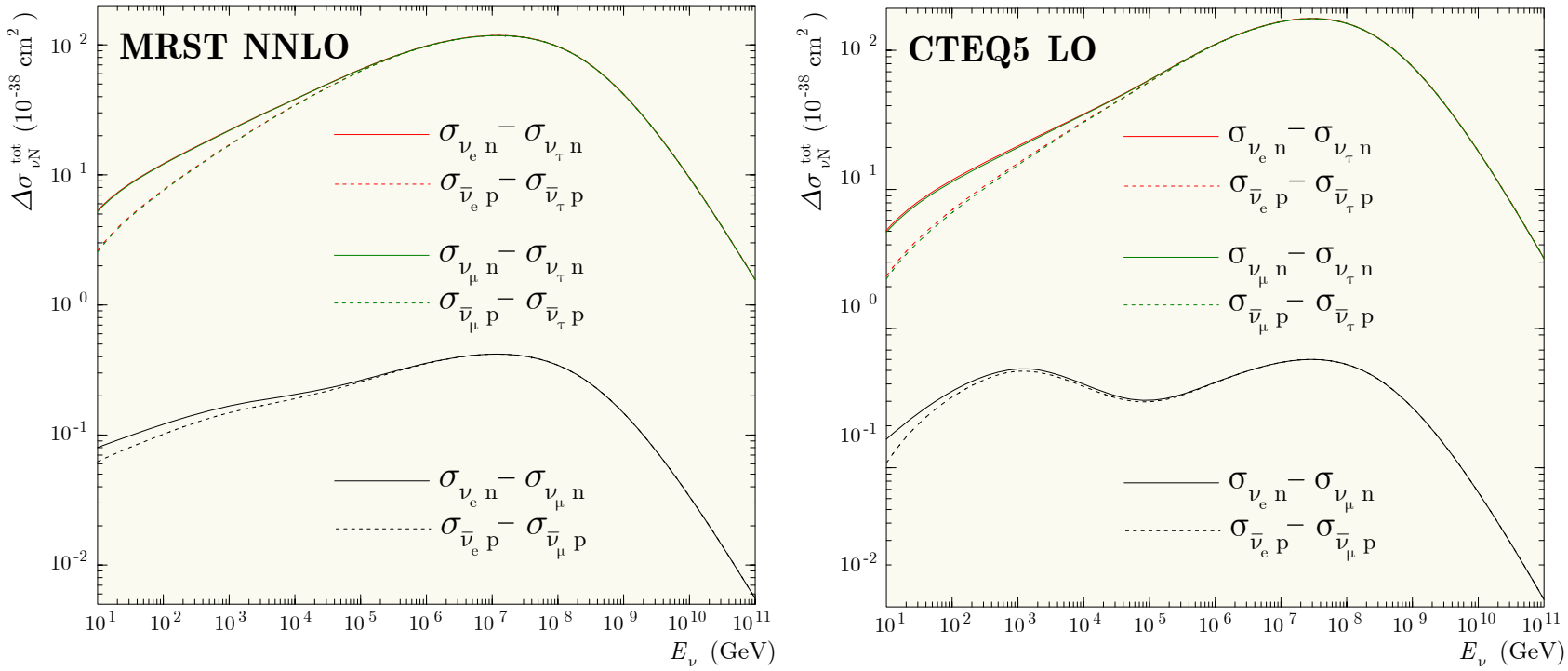

Figure 27: Differences between the total neutrino cross sections for proton and neutron targets evaluated with the MRST 2002 NNLO (left) and CTEQ 5-DIS LO (right) PDF models.

Indices of refraction

For $E_\nu \ll \min\left(m_{W,Z}^2/2m_A\right)$ and for an electroneutral nonpolarized cold medium, the q_R is energy independent. In the leading orders of the standard electroweak theory it is

$$q_R = \begin{cases} \frac{1}{2}V_0 Y_p \rho & \text{for } \alpha = e \text{ and } \beta = \mu \text{ or } \tau, \\ -\frac{1}{2}a_\tau V_0 \left(Y_p + b_\tau Y_n\right)\rho & \text{for } \alpha = \mu \text{ and } \beta = \tau, \\ \frac{1}{2}V_0 \left(Y_p - \frac{1}{2}Y_n\right)\rho & \text{for } \alpha = e \text{ and } \beta = s, \\ \frac{1}{4}V_0 Y_n \rho & \text{for } \alpha = \mu \text{ or } \tau \text{ and } \beta = s, \end{cases}$$

where

$$V_0 = \sqrt{2}G_F N_0 \simeq 7.63 \times 10^{-14} \text{ eV} \quad \left(L_0 = \frac{2\pi}{V_0} \simeq 1.62 \times 10^4 \text{ km} \sim D_\oplus\right),$$

$$a_\tau = \frac{3\alpha r_\tau \left[\ln(1/r_\tau) - 1\right]}{4\pi \sin^2\theta_W} \simeq 2.44 \times 10^{-5}, \quad b_\tau = \frac{\ln(1/r_\tau) - 2/3}{\ln(1/r_\tau) - 1} \simeq 1.05,$$

α is the fine-structure constant, θ_W is the weak-mixing angle and $r_\tau = (m_\tau/m_W)^2$.

Notes:

- For an isoscalar medium the $|q_R|$ is of the same order of magnitude for any pair of flavors but $\nu_\mu - \nu_\tau$.
- For an isoscalar medium $q_R^{(\nu_\mu - \nu_\tau)}/q_R^{(\nu_e - \nu_\mu)} \approx -5 \times 10^{-5}$.

- For certain regions of a neutron-rich medium the value of $q_R^{(\nu_e - \nu_s)}$ may become vanishingly small. In this case, the one-loop radiative corrections must be taken into account.
- For very high energies the q_R have to be corrected for the gauge boson propagators and strong-interaction effects.

One can expect $|q_R|$ to be either an energy-independent or decreasing function for any pair of mixed neutrino flavors. On the other hand, there are several cases of much current interest when $|q_I|$ either increases with energy without bound (mixing between active and sterile neutrino states) or has a broad or sharp maximum (as for $\nu_\mu - \nu_\tau$ or $\overline{\nu}_e - \overline{\nu}_\mu$ mixings, respectively).

Numerical estimations suggest that for every of these cases there is an energy range in which q_R and q_I are comparable in magnitude. Since $q_R \propto \rho$ and $q_I \propto$ and are dependent upon the composition of the medium (Y_A) there may exist some more specific situations, when

$$|q_R| \sim |q_I| \sim |\Delta|$$

or even

$$|q_R| \sim |\Delta_c| \quad \text{and} \quad |q_I| \sim |\Delta_s| \,.$$

If this is the case, the refraction, absorption and mixing become interestingly superimposed.

Eigenproblem and mixing matrix in matter

Eigenvalues

The matrix $\mathbf{H}(t)$ has two complex instantaneous eigenvalues, $\varepsilon(t)$ and $-\varepsilon(t)$, with $\varepsilon = \varepsilon_R + i\varepsilon_I$ satisfying the characteristic equation

$$\varepsilon^2 = (q - q_+)\,(q - q_-)\,,$$

where $q_\pm = \Delta_c \pm i\Delta_s = \Delta e^{\pm 2i\theta}$. The solution is

$$\varepsilon_R^2 = \frac{1}{2}\left(\varepsilon_0^2 - q_I^2\right) + \frac{1}{2}\sqrt{\left(\varepsilon_0^2 - q_I^2\right)^2 + 4q_I^2\left(\varepsilon_0^2 - \Delta_s^2\right)},$$

$$\varepsilon_I = \frac{q_I\,(q_R - \Delta_c)}{\varepsilon_R} \quad \text{(provided } q_R \neq \Delta_c)\,,$$

with

$$\varepsilon_0 = \sqrt{\Delta^2 - 2\Delta_c q_R + q_R^2} \geq |\Delta_s|, \qquad \text{sign}\,(\varepsilon_R) \stackrel{\text{def}}{=} \text{sign}(\Delta) \equiv \zeta.$$

(At that choice $\varepsilon = \Delta$ for vacuum and $\varepsilon = \zeta\varepsilon_0$ if $q_I = 0$.)

In the vicinity of the MSW resonance, $q_R = q_R(t_\star) = \Delta_c$

$$\lim_{q_R \to \Delta_c \pm 0} \varepsilon_R = \Delta_s \sqrt{\max\left(1 - \Delta_I^2/\Delta_s^2, 0\right)},$$

$$\lim_{q_R \to \Delta_c \pm 0} \varepsilon_I = \pm\zeta\Delta_I \sqrt{\max\left(1 - \Delta_s^2/\Delta_I^2, 0\right)},$$

where $\Delta_I = q_I(t_\star)$. Therefore the resonance value of $|\varepsilon_R|$ (which is inversely proportional to the neutrino oscillation length in matter) is always smaller than the conventional MSW value $|\Delta_s|$ and *vanishes* if $\Delta_I^2 < \Delta_s^2$ (ε_I remains finite in this case). In neutrino transition through the region of resonance density $\rho = \rho(t_\star)$, ε_I undergoes discontinuous jump while ε_R remains continuous. The corresponding cuts in the q plane are placed outside the circle $|q| \leq |\Delta|$. If $\Delta_I^2 > \Delta_s^2$, the imaginary part of ε vanishes while the real part remains finite.

A distinctive feature of the characteristic equation is the existence of two mutually conjugate "super-resonance" points $q_\pm$ in which ε vanishes giving rise to the total degeneracy of the levels of the system (impossible in the "standard MSW" solution). Certainly, the behavior of the system in the vicinity of these points must be dramatically different from the conventional pattern.

The "super-resonance" conditions are physically realizable for various meaningful mixing scenarios.

Eigenstates

In order to simplify the solution to the eigenstate problem we'll assume that the phase trajectory $q = q(t)$ does not cross the points $q_\pm$ at any t. In non-Hermitian quantum dynamics one has to consider the two pairs of instantaneous eigenvectors $|\Psi_\pm\rangle$ and $|\overline{\Psi}_\pm\rangle$ which obey the relations

$$\mathbf{H}|\Psi_\pm\rangle = \pm\,\varepsilon|\Psi_\pm\rangle \quad \text{and} \quad \mathbf{H}^\dagger|\overline{\Psi}_\pm\rangle = \pm\,\varepsilon^*|\overline{\Psi}_\pm\rangle. \tag{18}$$

and (for $q \neq q_\pm$) form a complete biorthogonal and biorthonormal set,

$$\langle\overline{\Psi}_\pm|\Psi_\pm\rangle = 1, \quad \langle\overline{\Psi}_\pm|\Psi_\mp\rangle = 0, \quad |\Psi_+\rangle\langle\overline{\Psi}_+| + |\Psi_-\rangle\langle\overline{\Psi}_-| = \mathbf{1}.$$

Therefore, the eigenvectors are defined up to a gauge transformation

$$|\Psi_\pm\rangle \mapsto e^{if_\pm}|\Psi_\pm\rangle, \quad |\overline{\Psi}_\pm\rangle \mapsto e^{-if_\pm^*}|\overline{\Psi}_\pm\rangle,$$

with arbitrary complex functions $f_\pm(t)$ such that $\mathrm{Im}\,(f_\pm)$ vanish as $q = 0$.[a] Thus it is sufficient to find any particular solution of Eqs. (18). Taking into account that $\mathbf{H}^\dagger = \mathbf{H}^*$, we may set $|\overline{\Psi}_\pm\rangle = |\Psi_\pm^*\rangle$ and hence the eigenvectors can be found from the identity

$$\mathbf{H} = \varepsilon|\Psi_+\rangle\langle\Psi_+^*| - \varepsilon|\Psi_-\rangle\langle\Psi_-^*|.$$

[a] For our aims, the class of the gauge functions may be restricted without loss of generality by the condition $f_\pm|_{q=0} = 0$.

Setting $|\Psi_\pm\rangle = (v_\pm, \pm v_\mp)^T$ we arrive at the equations

$$v_\pm^2 = \frac{\varepsilon \pm (q - \Delta_c)}{2\varepsilon}, \quad v_+ v_- = \frac{\Delta_s}{2\varepsilon},$$

a particular solution of which can be written as

$$v_+ = \sqrt{\left|\frac{\varepsilon + q - \Delta_c}{2\varepsilon}\right|}\, e^{i(\varphi-\psi)/2},$$

$$v_- = \zeta\sqrt{\left|\frac{\varepsilon - q + \Delta_c}{2\varepsilon}\right|}\, e^{i(-\varphi-\psi)/2}.$$

where

$$\varphi = \arg(\varepsilon + q - \Delta_c) = -\arg(\varepsilon - q + \Delta_c) = \arctan\left(\frac{q_I}{\varepsilon_R}\right),$$

$$\psi = \arg(\varepsilon) = \arctan\left(\frac{\varepsilon_I}{\varepsilon_R}\right),$$

and we have fixed the remaining gauge ambiguity by a comparison with the vacuum case.

Mixing angle in matter

It may be sometimes useful to define the complex mixing angle in matter $\Theta = \Theta_R + i\Theta_I$ by the relations

$$\sin\Theta = v_+ \quad \text{and} \quad \cos\Theta = v_-$$

or, equivalently,

$$\sin 2\Theta = \frac{\Delta_s}{\varepsilon}, \quad \cos 2\Theta = \frac{\Delta_c - q}{\varepsilon},$$

The real and imaginary parts of Θ are found to be

$$\mathrm{Re}(\Theta) \equiv \Theta_R = \frac{1}{2}\arctan\left[\frac{(q_I - \Delta_s)\,\varepsilon_R - (q_R - \Delta_c)\,\varepsilon_I}{(q_R - \Delta_c)\,\varepsilon_R + (q_I - \Delta_s)\,\varepsilon_I}\right],$$

$$\mathrm{Im}(\Theta) \equiv \Theta_I = \frac{1}{4}\ln\left[\frac{\varepsilon_R^2 + \varepsilon_I^2}{(q_R - \Delta_c)^2 + (q_I - \Delta_s)^2}\right].$$

$$\cos\Theta = \cos\Theta_R \cosh\Theta_I - i\sin\Theta_R \sinh\Theta_I,$$
$$\sin\Theta = \sin\Theta_R \cosh\Theta_I + i\cos\Theta_R \sinh\Theta_I.$$

Having regard to the prescription for the sign of ε_R, one can verify that $\Theta = \theta$ if $q = 0$ (vacuum case) and $\Theta = 0$ if $\Delta_s = 0$ (no mixing or $m_1^2 = m_2^2$). It is also clear that Θ becomes the standard MSW mixing angle with $\mathrm{Im}(\Theta) = 0$ when $q_I = 0$ ($\Lambda_\alpha = \Lambda_\beta$).

Mixing matrix in matter

In order to build up the solution to ME for the nondegenerated case one has to diagonalize the Hamiltonian. Generally a non-Hermitian matrix cannot be diagonalized by a single unitary transformation. But in our simple case this can be done by a complex orthogonal matrix (extended mixing matrix in matter)

$$\mathbf{U}_f = \mathbf{U}\exp(i\mathbf{f}),$$

where $\mathbf{f} = \mathrm{diag}\,(f_-, f_+)$ and

$$\mathbf{U} = (|\Psi_-\rangle, |\Psi_+\rangle) = \begin{pmatrix} v_- & v_+ \\ -v_+ & v_- \end{pmatrix} = \begin{pmatrix} \cos\Theta & \sin\Theta \\ -\sin\Theta & \cos\Theta \end{pmatrix}.$$

Properties of $\mathbf{U}$:

$$\mathbf{U}^T\mathbf{H}\mathbf{U} = \mathrm{diag}\,(-\varepsilon, \varepsilon),$$
$$\mathbf{U}^T\mathbf{U} = \mathbf{1},$$
$$\mathbf{U}|_{q=0} = \mathbf{V}.$$

From CE it follows that

$$\partial\varepsilon/\partial q = (q - \Delta_c)/\varepsilon$$

and thus

$$\frac{\partial v_\pm}{\partial q} = \pm\frac{\Delta_s^2 v_\mp}{2\varepsilon^2}.$$

We therefore have

$$i\mathbf{U}^T\dot{\mathbf{U}} = -\Omega\begin{pmatrix} 0 & -i \\ i & 0 \end{pmatrix} = -\Omega\boldsymbol{\sigma}_2,$$

where

$$\Omega = \frac{\dot{q}\Delta_s}{2\varepsilon^2} = \frac{i}{4}\frac{d}{dt}\ln\left(\frac{q - q_+}{q - q_-}\right).$$

Properties of $\mathbf{U}_f$:

$$\mathbf{U}_f^T\mathbf{H}\mathbf{U}_f = \mathsf{diag}\,(-\varepsilon, \varepsilon),$$
$$\mathbf{U}_f^T\mathbf{U}_f = \mathbf{1},$$
$$\mathbf{U}_f|_{q=0} = \mathbf{V},$$
$$i\mathbf{U}_f^T\dot{\mathbf{U}}_f = -\Omega e^{-i\mathbf{f}}\boldsymbol{\sigma}_2 e^{i\mathbf{f}} - \dot{\mathbf{f}}.$$

Adiabatic solution

Formal solution to ME in the most general form:

$$\widetilde{\mathbf{S}}(t) = \mathbf{U}_f(t) \exp\left[-i\mathbf{\Phi}(t)\right] \mathbf{X}_f(t) \mathbf{U}_f^T(0). \tag{19}$$

Here $\mathbf{\Phi}(t) = \mathrm{diag}\left(-\Phi(t), \Phi(t)\right)$ and $\Phi(t) = \Phi_R(t) + i\Phi_I(t)$ is the complex dynamical phase, defined by

$$\Phi_R(t) = \int_0^t \varepsilon_R(t')dt', \quad \Phi_I(t) = \int_0^t \varepsilon_I(t')dt',$$

and $\mathbf{X}_f(t)$ must satisfy the equation

$$i\dot{\mathbf{X}}_f(t) = \left[\Omega(t) e^{-i\mathbf{f}(t)} \mathbf{F}(t) e^{i\mathbf{f}(t)} + \dot{\mathbf{f}}(t)\right] \mathbf{X}_f(t), \quad \mathbf{X}_f(0) = \mathbf{1},$$

where

$$\mathbf{F}(t) = e^{i\mathbf{\Phi}(t)} \boldsymbol{\sigma}_2 e^{-i\mathbf{\Phi}(t)} = \begin{pmatrix} 0 & -ie^{-2i\Phi(t)} \\ ie^{2i\Phi(t)} & 0 \end{pmatrix}.$$

It can be proved now that the right side of Eq. (19) is gauge-invariant i.e. it does not depend on the unphysical complex phases $f_\pm(t)$. This crucial fact is closely related to the absence of the Abelian topological phases in the system under consideration.

Finally, we can put $f_\pm = 0$ in Eq. (19) and the result is

$$\widetilde{\mathbf{S}}(t) = \mathbf{U}(t) \exp\left[-i\mathbf{\Phi}(t)\right] \mathbf{X}(t)\mathbf{U}^T(0), \tag{20a}$$

$$i\dot{\mathbf{X}}(t) = \Omega(t)\mathbf{F}(t)\mathbf{X}(t), \quad \mathbf{X}(0) = \mathbf{1}. \tag{20b}$$

These equations, being equivalent to the ME, have nevertheless a restricted range of practical usage on account of poles and cuts as well as decaying and increasing exponents in the "Hamiltonian" $\Omega\mathbf{F}$.

Adiabatic theorem

The adiabatic theorem of Hermitian quantum mechanics can almost straightforwardly be extended to ME under the requirements:

(a) the potential q is a sufficiently smooth and slow function of t;

(b) the imaginary part of the dynamical phase is a bounded function i.e. $\lim_{t\to\infty} |\Phi_I(t)|$ is finite;

(c) the phase trajectory $q = q(t)$ is placed far from the singularities for any t.

The first requirement breaks down for a condensed medium with a sharp boundary or layered structure (like the Earth). If however the requirement (a) is valid inside each layer (t_i, t_{i+1}), the problem reduces to Eqs. (20) by applying the rule

$$\widetilde{\mathbf{S}}(t) \equiv \widetilde{\mathbf{S}}(t,0) = \widetilde{\mathbf{S}}\,(t,t_n)\ldots\widetilde{\mathbf{S}}\,(t_2,t_1)\,\widetilde{\mathbf{S}}\,(t_1,0),$$

where $\widetilde{\mathbf{S}}\,(t_{i+1},t_i)$ is the time-evolution operator for the i-th layer.

The requirement (b) alone is not too restrictive considering that for many astrophysical objects (like stars, galactic nuclei, jets and so on) the density ρ exponentially disappears to the periphery and, on the other hand, $\varepsilon_I \to 0$ as $\rho \to 0$. In this instance, the function $\Phi_I(t)$ must be t independent for sufficiently large t. But, in the case of a steep density profile, the requirements (a) and (b) may be inconsistent.

The important case of violation of the requirement (c) is the subject of a special study which is beyond the scope of this study.

It is interesting to note in this connection that, in the Hermitian case, a general adiabatic theorem has been proved without the traditional gap condition [J. E. Avron and A. Elgart, Commun. Math. Phys. **203** (1999) 445].

The solution

Presume that all necessary conditions do hold for $0 \leq t \leq T$. Then, in the adiabatic limit, we can put $\Omega = 0$ in Eq. (20b). Therefore $\mathbf{X} = \mathbf{1}$ and Eq. (20a) yields

$$\widetilde{S}_{\alpha\alpha}(t) = v_+(0)v_+(t)e^{-i\Phi(t)} + v_-(0)v_-(t)e^{i\Phi(t)},$$
$$\widetilde{S}_{\alpha\beta}(t) = v_-(0)v_+(t)e^{-i\Phi(t)} - v_+(0)v_-(t)e^{i\Phi(t)},$$
$$\widetilde{S}_{\beta\alpha}(t) = v_+(0)v_-(t)e^{-i\Phi(t)} - v_-(0)v_+(t)e^{i\Phi(t)},$$
$$\widetilde{S}_{\beta\beta}(t) = v_-(0)v_-(t)e^{-i\Phi(t)} + v_+(0)v_+(t)e^{i\Phi(t)},$$

Taking into account Eq. (17) we obtain the survival and transition probabilities:

$$
\begin{aligned}
P_{\alpha\alpha}(t) &= A(t)\left\{\left[I_+^+(t)e^{\Phi_I(t)} + I_-^-(t)e^{-\Phi_I(t)}\right]^2 - I^2(t)\sin^2\left[\Phi_R(t) - \varphi_+(t)\right]\right\},\\
P_{\alpha\beta}(t) &= A(t)\left\{\left[I_+^-(t)e^{\Phi_I(t)} - I_-^+(t)e^{-\Phi_I(t)}\right]^2 + I^2(t)\sin^2\left[\Phi_R(t) - \varphi_-(t)\right]\right\},\\
P_{\beta\alpha}(t) &= A(t)\left\{\left[I_-^+(t)e^{\Phi_I(t)} - I_+^-(t)e^{-\Phi_I(t)}\right]^2 + I^2(t)\sin^2\left[\Phi_R(t) + \varphi_-(t)\right]\right\},\\
P_{\beta\beta}(t) &= A(t)\left\{\left[I_-^-(t)e^{\Phi_I(t)} + I_+^+(t)e^{-\Phi_I(t)}\right]^2 - I^2(t)\sin^2\left[\Phi_R(t) + \varphi_+(t)\right]\right\},
\end{aligned}
\tag{21}
$$

where we have denoted for compactness

$$
I_\varsigma^{\varsigma'}(t) = |v_\varsigma(0)v_{\varsigma'}(t)| \qquad (\varsigma,\varsigma' = \pm),
$$

$$
\varphi_\pm(t) = \frac{\varphi(0) \pm \varphi(t)}{2},
$$

$$
I^2(t) = 4I_+^+(t)I_-^-(t) = 4I_+^-(t)I_-^+(t) = \frac{\Delta_s^2}{|\varepsilon(0)\varepsilon(t)|}.
$$

Limiting cases

In the event that the conditions

$$\left|\frac{1}{\Lambda_\beta(t)}-\frac{1}{\Lambda_\alpha(t)}\right| \ll 4\varepsilon_0(t) \quad \text{and} \quad t \ll \min\left[\Lambda_\alpha(t),\Lambda_\beta(t)\right]$$

are satisfied for any $t \in [0,T]$, the formulas (21) reduce to the standard MSW adiabatic solution

$$\left.\begin{aligned} P_{\alpha\alpha}(t) = P_{\beta\beta}(t) &= \frac{1}{2}\left[1+J(t)\right] - I_0^2(t)\sin^2\left[\Phi_0(t)\right], \\ P_{\alpha\beta}(t) = P_{\beta\alpha}(t) &= \frac{1}{2}\left[1-J(t)\right] + I_0^2(t)\sin^2\left[\Phi_0(t)\right], \end{aligned}\right\} \qquad \text{(MSW)}$$

where

$$J(t) = \frac{\Delta^2 - \Delta_c\left[q_R(0)+q_R(t)\right]+q_R(0)q_R(t)}{\varepsilon_0(0)\varepsilon_0(t)},$$

$$I_0^2(t) = \frac{\Delta_s^2}{\varepsilon_0(0)\varepsilon_0(t)}, \quad \Phi_0(t) = \int_0^t \varepsilon_0(t')dt'.$$

Needless to say either of the above conditions or both may be violated for sufficiently high neutrino energies and/or for thick media, resulting in radical differences between the two solutions. These differences are of obvious interest to high-energy neutrino astrophysics.

It is perhaps even more instructive to examine the distinctions between the general adiabatic solution (21) and its "classical limit"

$$\left.\begin{aligned} P_{\alpha\alpha}(t) &= \exp\left[-\int_0^t \frac{dt'}{\Lambda_\alpha(t')}\right], \quad P_{\alpha\beta}(t) = 0, \\ P_{\beta\beta}(t) &= \exp\left[-\int_0^t \frac{dt'}{\Lambda_\beta(t')}\right], \quad P_{\beta\alpha}(t) = 0, \end{aligned}\right\} \qquad (\Delta_s = 0)$$

which takes place either in the absence of mixing or for $m_1^2 = m_2^2$.

Note:

Considering that $\Omega \propto \Delta_s$, the classical limit is the exact solution to the master equation (for $\Delta_s = 0$). Therefore it can be derived directly from Eq. (16). To make certain that the adiabatic solution has correct classical limit, the following relations are useful:

$$\lim_{\Delta_s \to 0} \varepsilon(t) = \zeta\zeta_R \left[q(t) - \Delta_c\right] \quad \text{and} \quad \lim_{\Delta_s \to 0} |v_\pm(t)|^2 = \frac{1}{2}\left(\zeta\zeta_R \pm 1\right),$$

where $\zeta_R = \text{sign}\left[q_R(t) - \Delta_c\right]$.

Matter of constant density and composition

In this simple case, the adiabatic approximation becomes exact and thus free from the above-mentioned conceptual difficulties. For definiteness sake we assume $\Lambda_\alpha < \Lambda_\beta$ (and thus $q_I < 0$) from here. The opposite case can be considered in a similar way. Let's denote

$$\frac{1}{\Lambda_\pm} = \frac{1}{2}\left(\frac{1}{\Lambda_\alpha} + \frac{1}{\Lambda_\beta}\right) \pm \frac{\xi}{2}\left(\frac{1}{\Lambda_\alpha} - \frac{1}{\Lambda_\beta}\right),$$

$$I_\pm^2 = \frac{1}{4}\left(1 + \frac{\varepsilon_0^2 + q_I^2 - \Delta_s^2}{\varepsilon_R^2 + \varepsilon_I^2}\right) \pm \frac{\xi}{2}\left(\frac{\varepsilon_R^2 + q_I^2}{\varepsilon_R^2 + \varepsilon_I^2}\right),$$

$$L = \frac{\pi}{|\varepsilon_R|} \quad \text{and} \quad \xi = \left|\frac{q_R - \Delta_c}{\varepsilon_R}\right|.$$

As is easy to see,

$$I_\pm^\pm = \begin{cases} I_\pm & \text{if} \quad \text{sign}\,(q_R - \Delta_c) = +\zeta, \\ I_\mp & \text{if} \quad \text{sign}\,(q_R - \Delta_c) = -\zeta, \end{cases}$$

$$I_+^- = I_-^+ = \sqrt{I_+ I_-} = \frac{I}{2} = \left|\frac{\Delta_s}{2\varepsilon}\right| \quad \text{and} \quad \text{sign}(\varphi) = -\zeta.$$

By applying these identities the neutrino oscillation probabilities can be written as

$$P_{\alpha\alpha}(t) = \left(I_+ e^{-t/2\Lambda_+} + I_- e^{-t/2\Lambda_-}\right)^2 - I^2 e^{-t/\Lambda} \sin^2\left(\frac{\pi t}{L} + |\varphi|\right),$$

$$P_{\beta\beta}(t) = \left(I_- e^{-t/2\Lambda_+} + I_+ e^{-t/2\Lambda_-}\right)^2 - I^2 e^{-t/\Lambda} \sin^2\left(\frac{\pi t}{L} - |\varphi|\right),$$

$$P_{\alpha\beta}(t) = P_{\beta\alpha}(t) = \frac{1}{4} I^2 \left(e^{-t/2\Lambda_-} - e^{-t/2\Lambda_+}\right)^2 + I^2 e^{-t/\Lambda} \sin^2\left(\frac{\pi t}{L}\right).$$

The difference between the survival probabilities for ν_α and ν_β is

$$P_{\alpha\alpha}(t) - P_{\beta\beta}(t) = -\zeta \mathrm{Re}\left(\frac{q - \Delta_c}{\varepsilon}\right)\left(e^{-t/2\Lambda_-} - e^{-t/2\Lambda_+}\right)$$
$$+ I^2 e^{-t/\Lambda} \sin\varphi \sin\left(\frac{2\pi t}{L}\right).$$

Case $|q| \gtrsim |\Delta_s|$

Let's examine the case when Λ_+ and Λ_- are vastly different in magnitude. This will be true when $\Lambda_\beta \gg \Lambda_\alpha$ and the factor ξ is not too small. The second condition holds if q_R is away from the MSW resonance value Δ_c and the following dimensionless parameter

$$\varkappa = \frac{\Delta_s}{|q|} \approx 0.033 \times \sin 2\theta \left(\frac{\Delta m^2}{10^{-3}\ \text{eV}^2}\right)\left(\frac{100\ \text{GeV}}{E_\nu}\right)\left(\frac{V_0}{|q|}\right)$$

is sufficiently small. In fact we assume $|\varkappa| \lesssim 1$ and impose no specific restriction for the ratio q_R/q_I. This spans several possibilities:

- $\star$ small Δm^2,
- $\star$ small mixing angle,
- $\star$ high energy,
- $\star$ high matter density.

The last two possibilities are of special interest because the inequality $|\varkappa| \lesssim 1$ may be fulfilled for a wide range of the mixing parameters Δm^2 and θ by changing E_ν and/or ρ. In other words, this condition is by no means artificial or too restrictive.

After elementary while a bit tedious calculations we obtain

$$\xi = 1 - \frac{1}{2}\varkappa^2 + \mathcal{O}\left(\varkappa^3\right), \quad I^2 = \varkappa^2 + \mathcal{O}\left(\varkappa^3\right),$$

$$I_+ = 1 + \mathcal{O}\left(\varkappa^2\right), \quad I_- = \frac{1}{4}\varkappa^2 + \mathcal{O}\left(\varkappa^3\right);$$

$$\Lambda \approx 2\Lambda_\alpha,$$
$$\Lambda_+ \approx \left(1 + \frac{\varkappa^2}{4}\right)\Lambda_\alpha \approx \Lambda_\alpha,$$
$$\Lambda_- \approx \left(\frac{4}{\varkappa^2}\right)\Lambda_\alpha \gg \Lambda_\alpha.$$

Due to the wide spread among the length/time scales $\Lambda_\pm$, Λ and L as well as among the amplitudes $I_\pm$ and I, the regimes of neutrino oscillations are quite diverse for different ranges of variable t.

With reference to Figs. 28–31, one can see a regular gradation from slow (at $t \lesssim \Lambda_\mu$) to very fast (at $t \gtrsim \Lambda_\mu$) neutrino oscillations followed by the asymptotic nonoscillatory behavior:

$$P_{\mu\mu}(t) \simeq \frac{\varkappa^4}{16} e^{-t/\Lambda_-},$$
$$P_{ss}(t) \simeq e^{-t/\Lambda_-},$$
$$P_{\mu s}(t) = P_{s\mu}(t) \simeq \frac{\varkappa^2}{4} e^{-t/\Lambda_-}.$$

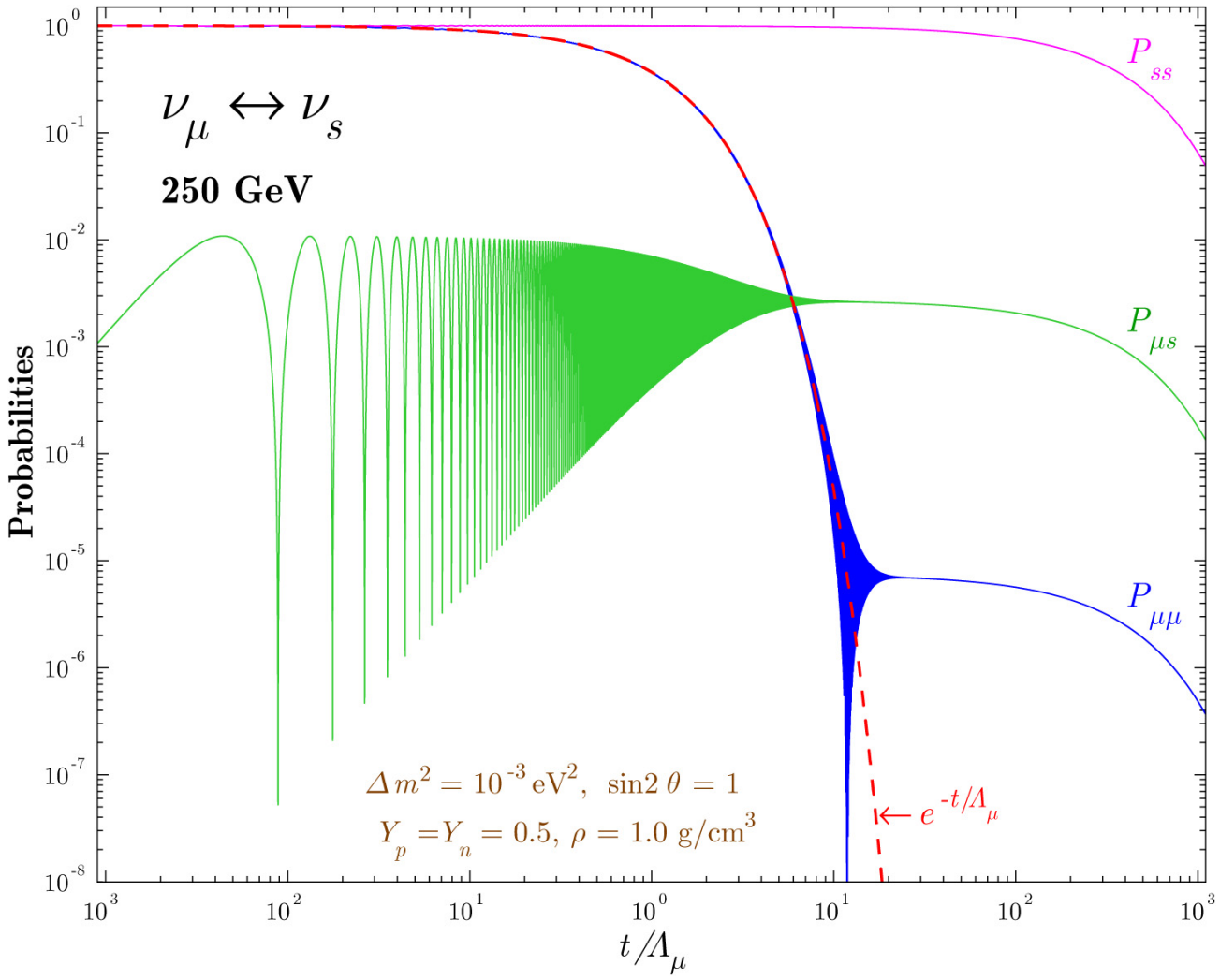

Figure 28: Survival and transition probabilities for $\nu_\mu \leftrightarrow \nu_s$ oscillations ($E_\nu = 250$ GeV, $\rho = 1$ g/cm^3).

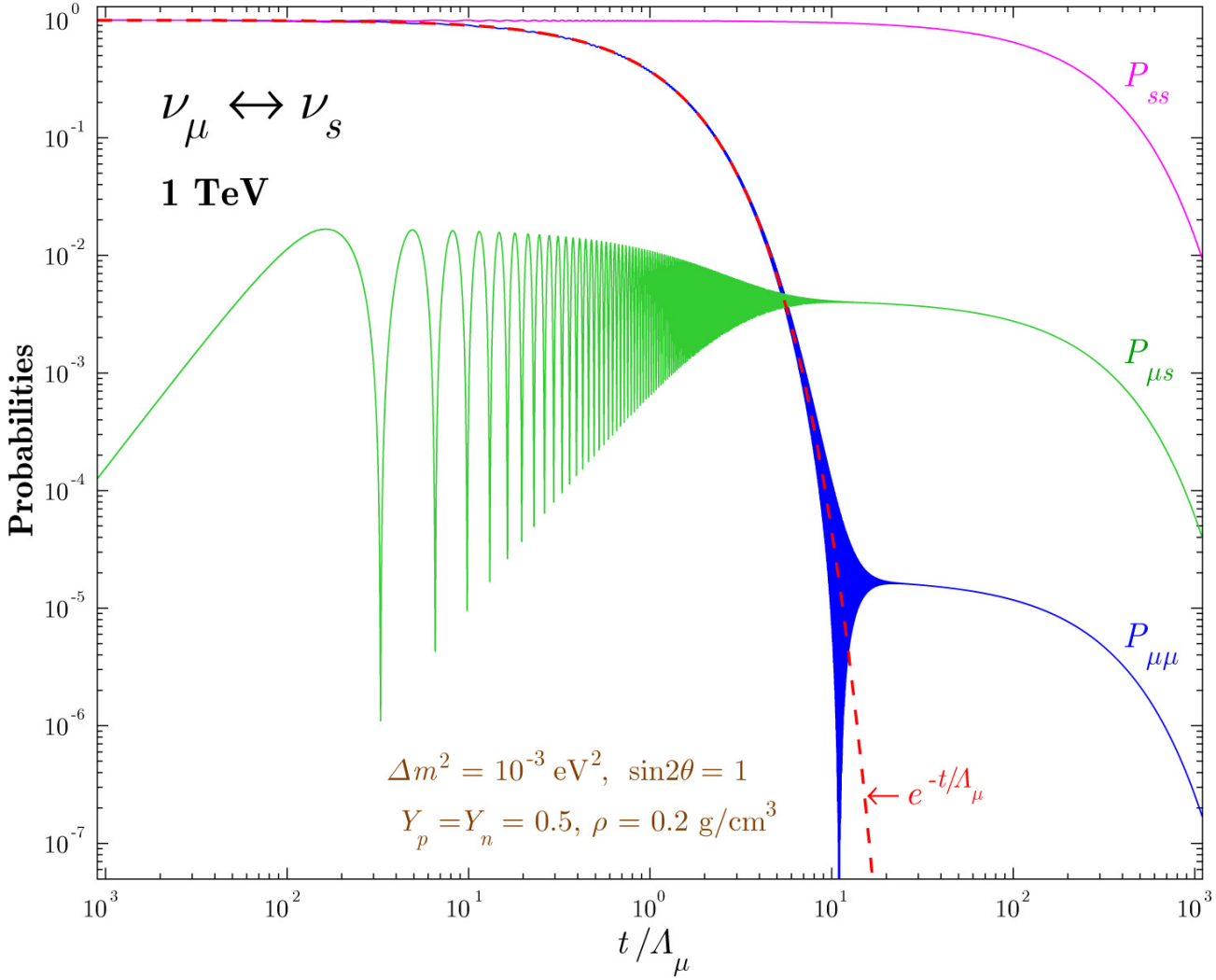

Figure 29: Survival and transition probabilities for $\nu_\mu \leftrightarrow \nu_s$ oscillations ($E_\nu = 1000$ GeV, $\rho = 0.2$ g/cm^3).

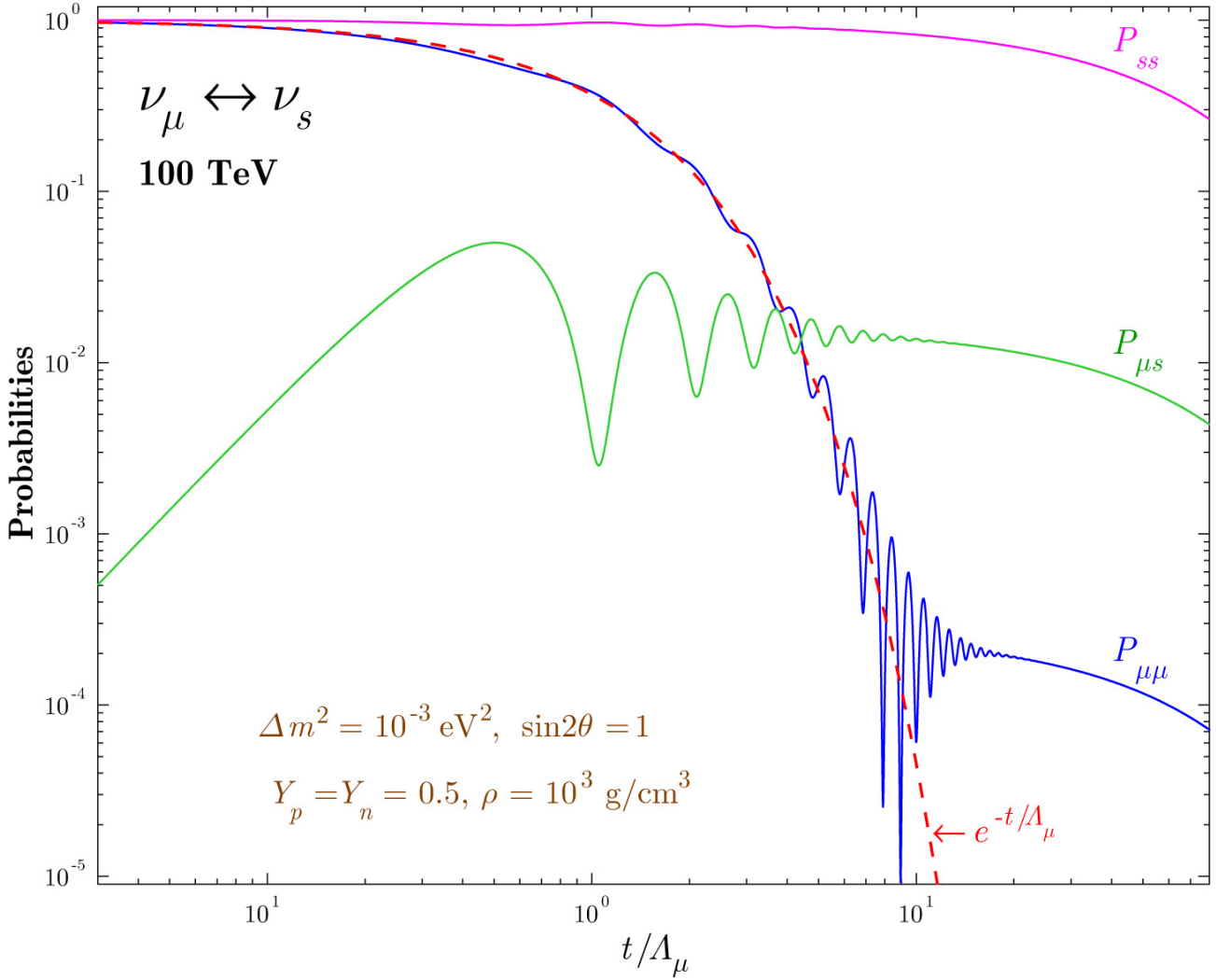

Figure 30: Survival and transition probabilities for $\nu_\mu \leftrightarrow \nu_s$ oscillations ($E_\nu = 100$ TeV, $\rho = 10^{-3}$ g/cm^3).

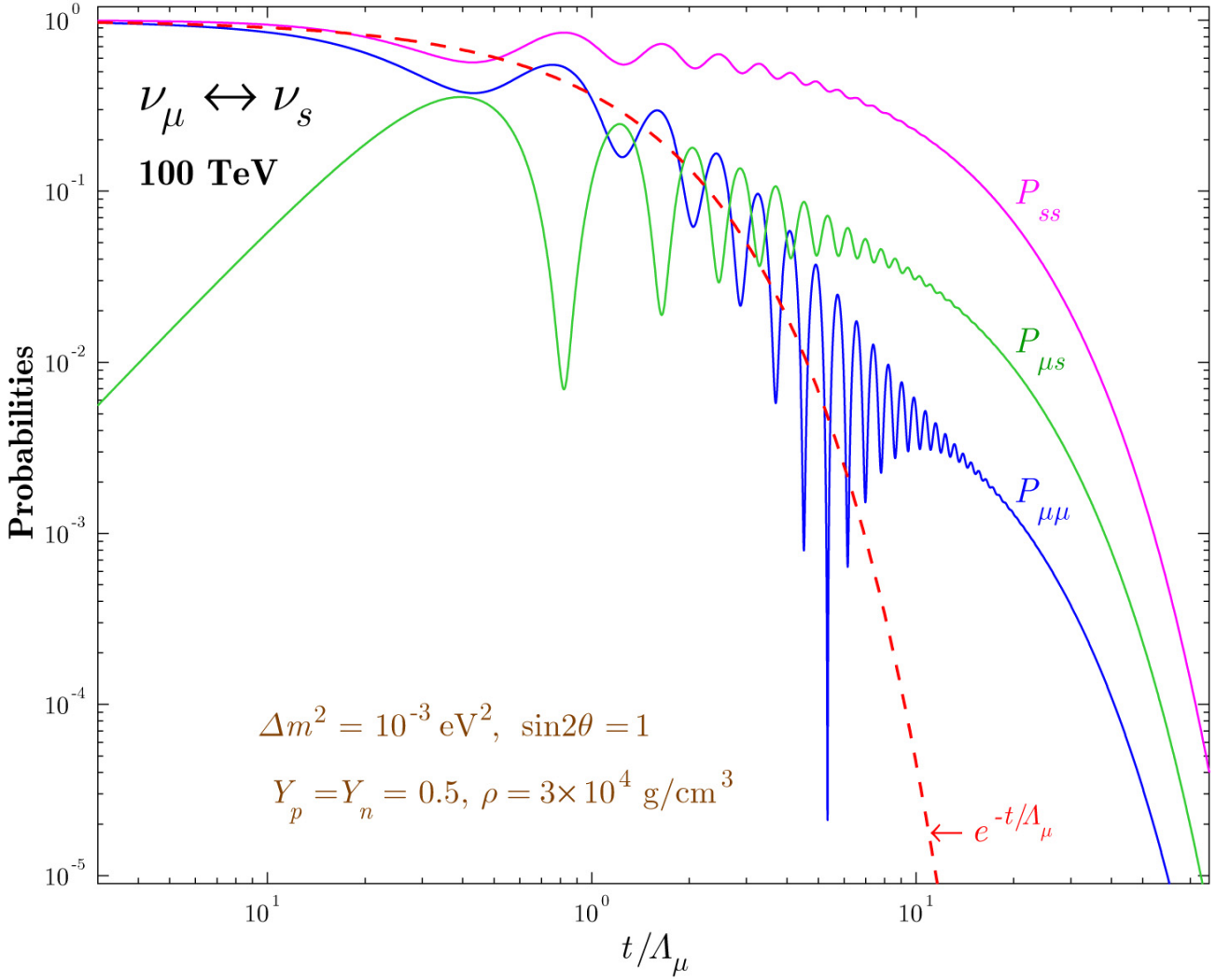

Figure 31: Survival and transition probabilities for $\nu_\mu \leftrightarrow \nu_s$ oscillations ($E_\nu = 100$ TeV, $\rho = 3 \times 10^{-4}$ g/cm^3).

Degenerate case

The consideration must be completed for the case of degeneracy. Due to the condition $q_I < 0$, the density and composition of the "degenerate environment" are fine-tuned in such a way that

$$q = q_{-\zeta} = \Delta_c - i\,|\Delta_s|.$$

The simplest way is in coming back to the master equation. Indeed, in the limit of $q = q_{-\zeta}$, the Hamiltonian reduces to

$$\mathbf{H} = |\Delta_s| \begin{pmatrix} -i & \zeta \\ \zeta & i \end{pmatrix} \equiv |\Delta_s|\,\mathbf{h}_\zeta.$$

Considering that $\mathbf{h}_\zeta^2 = \mathbf{0}$, we promptly arrive at the solution of ME:

$$\widetilde{\mathbf{S}}(t) = \mathbf{1} - it\,|\Delta_s|\,\mathbf{h}_\zeta$$

and thus

$$\begin{aligned} P_{\alpha\alpha}(t) &= (1 - |\Delta_s|\,t)^2\, e^{-t/\Lambda}, \\ P_{\beta\beta}(t) &= (1 + |\Delta_s|\,t)^2\, e^{-t/\Lambda}, \\ P_{\alpha\beta}(t) &= P_{\beta\alpha}(t) = (\Delta_s t)^2\, e^{-t/\Lambda}. \end{aligned}$$

Since $1/\Lambda_\beta = 1/\Lambda_\alpha - 4\,|\Delta_s|$, the necessary condition for the total degeneration is $4\Lambda_\alpha\,|\Delta_s| \leq 1$ and thus

$$1/\Lambda = 1/\Lambda_\alpha - 2\,|\Delta_s| \geq 2\,|\Delta_s|.$$

The equality only occurs when ν_β is sterile.

The degenerate solution must be compared with the standard MSW solution

$$\left.\begin{aligned} P_{\alpha\alpha}(t) = P_{ss}(t) &= \frac{1}{2}\,[1 + \cos\,(2\Delta_s t)], \\ P_{\alpha s}(t) = P_{s\alpha}(t) &= \frac{1}{2}\,[1 - \cos\,(2\Delta_s t)], \end{aligned}\right\} \qquad \text{(MSW)}$$

and with the classical penetration coefficient

$$\exp\,(-t/\Lambda_\alpha)$$

(with $1/\Lambda_\alpha$ numerically equal to $4\,|\Delta_s|$) relevant to the transport of unmixed active neutrinos through the same environment.

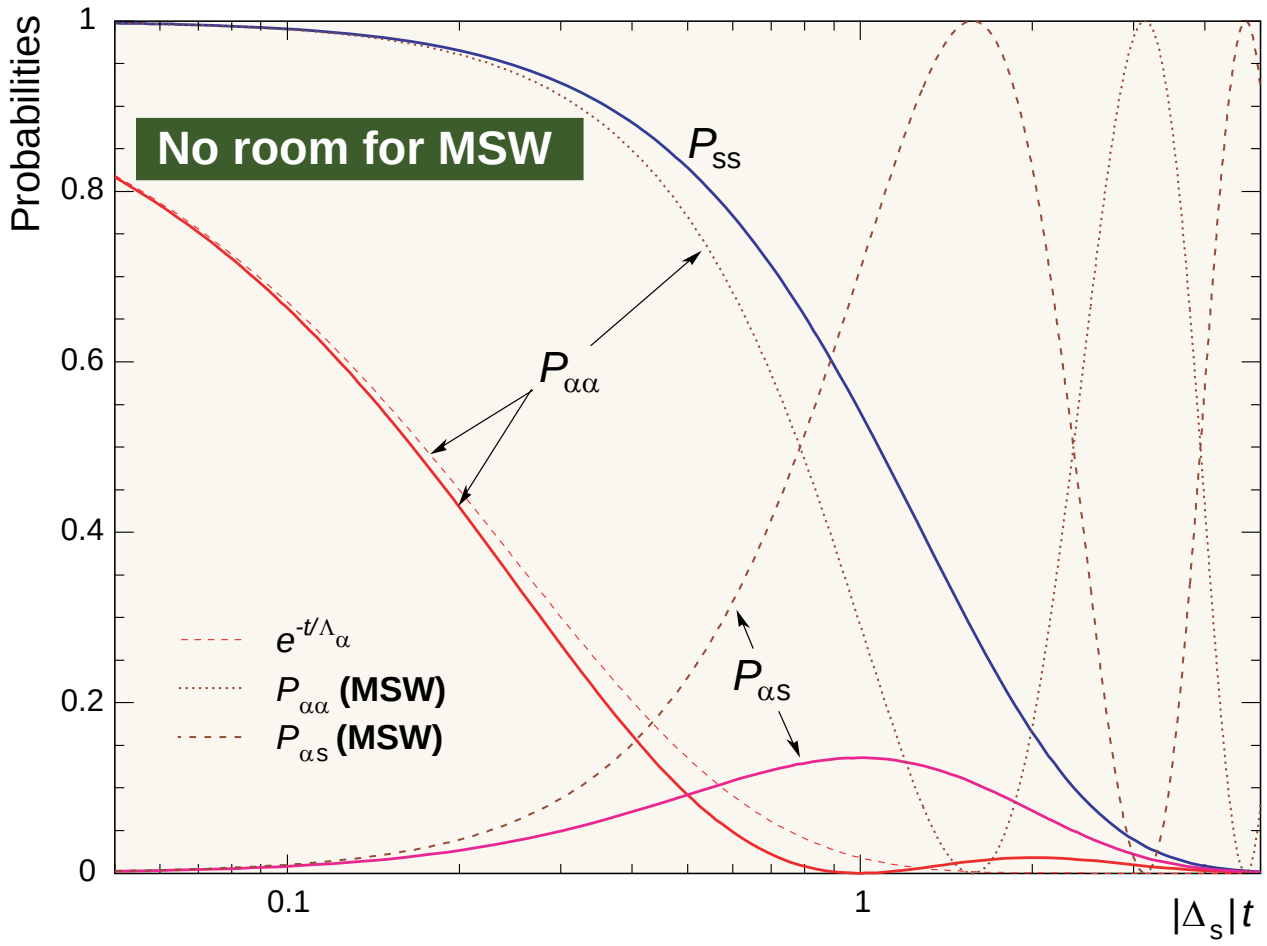

Figure 32: Survival and transition probabilities for $\nu_\alpha \leftrightarrow \nu_s$ oscillations in the case of degeneracy ($q = q_{-\zeta}$). The standard MSW probabilities (dotted and dash-dotted curves) together with the penetration coefficient for unmixed ν_α (dashed curve) are also shown.

Conclusions

We have considered, on the basis of the MSW evolution equation with complex indices of refraction, the conjoint effects of neutrino mixing, refraction and absorption on high-energy neutrino propagation through matter. The adiabatic solution with correct asymptotics in the standard MSW and classical limits has been derived. In the general case the adiabatic behavior is very different from the conventional limiting cases.

A noteworthy example is given by the active-to-sterile neutrino mixing. It has been demonstrated that, under proper conditions, the survival probability of active neutrinos propagating through a very thick medium of constant density may become many orders of magnitude larger than it would be in the absence of mixing. The quantitative characteristics of this phenomenon are highly responsive to changes in density and composition of the medium as well as to neutrino energy and mixing parameters.

Considering a great variety of latent astrophysical sources of high-energy neutrinos, the effect may open a new window for observational neutrino astrophysics.